



Contents lists available at ScienceDirect

Saudi Pharmaceutical Journal

journal homepage: www.sciencedirect.com

Original article

Single-step green synthesis of gold conjugated polyphenol nanoparticle using extracts of Saudi's myrrh: Their characterization, molecular docking and essential biological applications

Najlaa S. Al-Radadi

Department of Chemistry, Faculty of Science, Taibah University, P.O. Box 30002, Al-Madinah Al-Munawarah 14177, Saudi Arabia

ARTICLE INFO

Article history:

Received 7 May 2022

Accepted 25 June 2022

Available online 3 July 2022

Keywords:

Gold NPs

Commiphora myrrh

Antioxidant

Anticancer

Anti-inflammatory

Antidiabetic

Antibiotic

ABSTRACT

The progress in the innovative nanocrystal synthesis process by using environmentally benign and low-priced nontoxic chemicals, solvents, and renewable sources remains a challenging task for researchers worldwide. The majority of the existing synthesis techniques engage in the potentially dangerous, for either human health or the environment. Current investigation has been centered on green synthesis processes to create novel nanomaterials, which are eco-friendly as well as safer for sustainable marketable feasibility. The current work provides the green synthesis method for gold nanoparticle (GNPs) synthesis using *Commiphora myrrh* (*C.myrrh*) extract. This simple method includes 6 ml of $\text{HAuCl}_4 \cdot 3\text{H}_2\text{O}$ treated with 4 ml *C.myrrh* extract having pH 4.5 after 80 min at 25 °C temperature. In this novel method, green synthesized GNPs characterized by UV-Vis, X-ray diffraction spectroscopy (XRD), zeta potential, fourier transform infrared (FT-IR), high-resolution transmission electron microscopy (HR-TEM), energy dispersive X-ray spectroscopy (EDXA), and dynamic light scattering (DLS). During the development successful antioxidant assay, the DPPH assay was applied. The cell toxicity of green synthesized GNPs was evaluated following an MTT assay against HCT-116 (colon cancer) and MCF-7 (breast cancer).

Besides molecular docking in the δ -elemene for inhibitor to VEGFR-2 domain revealed more negative docking score (−3.976) which is an excellent binding affinity to the *C.myrrh*@GNP. The synthesized GNPs showed antidiabetic, antibiotic, and antibacterial properties and anti-inflammatory inhibition against inhibiting COX-1, and COX-2 enzymes. In addition, molecular docking by Lindrestrene (−3.806) and Furanoesdesma-1,3-dien (−3.912) against COX1 and COX2 respectively showed strong binding affinity. The molecular docking study evidenced the anti-inflammatory and cell toxicity study.

© 2022 The Author(s). Published by Elsevier B.V. on behalf of King Saud University. This is an open access article under the CC BY-NC-ND license (<http://creativecommons.org/licenses/by-nc-nd/4.0/>).

1. Introduction

Nanotechnology is a scientific study of properties and the extent of response capacity in addition to the directing materials on the molecular and atomic scale ranging from 1 to 100 nm. Despite the small scale or size of these materials (Kim et al., 2016), they can help in solving some complicated humanity problems (Abdelbasir and Shalan, 2019; Li et al., 2022; Liao et al.,

2021; Qiu et al., 2021; Yang et al., 2021; Yue et al., 2021). Currently, nanotechnology is renowned as a reputable progressive field having an extensive choice of applications including pharmaceutical and further industries. Metal nanoparticle production has gained growing concentration owing to its broad array of exercises in a variety of areas of medicine, electronics, and energy, (Doroudian et al., 2021; Kamat et al., 2021; Khalaf et al., 2021; Liang and Liang, 2021; Neha et al., 2021). Additionally, last decade, metal oxide nanoparticles also proved to be the subject of wide research, owing to their different application in many scientific areas (Aziz et al., 2015; Gan et al., 2019; Lee et al., 2020; Liu et al., 2019; Xue et al., 2017; Yang et al., 2018; Zhou et al., 2019), metal oxide (Faisal et al., 2021; Dizaj et al., 2014; Falcaro et al., 2016; Fernández-García and Rodríguez, 2007; Stoimenov et al., 2002; Franke et al., 2006). Nano-sized materials have been broadly used mainly considering their countless applications in different fields including chemical, physical

E-mail address: nsa@taibahu.edu.sa

Peer review under responsibility of King Saud University.



Production and hosting by Elsevier

<https://doi.org/10.1016/j.jsps.2022.06.028>

1319-0164/© 2022 The Author(s). Published by Elsevier B.V. on behalf of King Saud University.

This is an open access article under the CC BY-NC-ND license (<http://creativecommons.org/licenses/by-nc-nd/4.0/>).

and biological (Al Jahdaly et al., 2021; ranke et al., 2006; Nikam et al., 2018; Richter et al., 2010; De et al., 2008; Llop et al., 2014). Liquid metal nanoparticles are created from noble metals like Pt (Al-Radadi, 2019; Al-Radadi and Adam, 2020), Au (Dreaden et al., 2012; Sperling et al., 2008), and Ag (Al-Radadi and Abu-Dief, 2022; Abdullah et al., 2021; Al-Radadi, 2018; Al-Radadi and Al-Youbi, 2018a; Kaviya et al., 2011). Nanoparticles (denoted to NPs) showed excellent potential seeing that antimicrobial (Al-Radadi, 2022a; Behzad et al., 2021; Siegel et al., 2013), antioxidant (Desai et al., 2020; Zhang et al., 2018), anti-inflammatory agents (Sengupta et al., 2018), antidiabetic (Nirmala Grace and Pandian, 2007), anti-Alzheimer (Al-Radadi, 2022b; Al-Radadi et al., 2022) and anti-cancer (Al-Radadi, 2022c; Jain et al., 2007) having a strong capability of retarding the growth of unnecessary and injurious bacteria causing threatening disease. Gold nanoparticles (further termed as GNPs) have attracted lots of interest among noble metals due to their outstanding physicochemical and optical features, which can be broadly exploited in severe domain names of human activity (Al-Radadi, 2021a; Al-Radadi and Al-Youbi, 2018b). GNPs can in addition exhibit antimicrobial (Zhang et al., 2015), antioxidant potential (Al-Radadi, 2021b), and catalysis (Aswathy Aromal and Philip, 2012; Ramakrishna et al., 2016). GNPs are highly sensitive (Chen et al., 2008), stable (Balasubramanian et al., 2010), highly reliable, and less toxic (Lasagna-Reeves et al., 2010) than additional metal NPs.

However, a crucial asset of GNPs is their biocompatibility with living creatures building them broadly utilized within biomedical applications, drug delivery, sensor and diagnosis, and bio-imaging, (Kumar et al., 2011; Malathi et al., 2013). GNPs derived from natural sources have shown to be effective against a variety of uncontrolled growing cells *i.e.* cancer cell types (Khandanlou et al., 2018; Parida et al., 2014; Singh et al., 2019). As a result of widespread toxic concerns connected with chemical and physical processes, the eco-friendly 'green' synthesis of nano-sized materials has been a crucial and popular topic in support of material research in recent years (Albrecht et al., 2006; Khan, 2020). Plants are favored over some other organic procedures due to the fact they take away the requirement of retaining cell culture (David et al., 2014; Eccles, 1999).

The plant-intervened engineered approach (Al-Radadi, 2022c), is a significant procedure that can be helpfully made and engineered (Rajeshkumar and Bharath, 2017), the utilization of extracellular extract was viewed as more powerful and proficient in controlling the size, shape, and dispersity of the NPs (David et al., 2014; Narayanan and Sakthivel, 2011; Udayasoorian et al., 2011), therefore it is observed a typical plant referred to in old stories medication as "myrrh" is one of the most widely recognized spices in Saudi Arabia. *Commiphora myrrh* (*C. myrrh*) has a place with the class *Commiphora* and the family *Burseraceae* (Sheir et al., 2001; Su et al., 2011). *C. molmol* Engler (*Burseraceae*) is local to Madagascar, the Arabian islands, and India (Ben-Yehoshua and Borowitz, 2012). It is one of the best homegrown medications on the planet for sore throats, ulcers, and gum disease (Khalil et al., 2020). *C. molmol* Engler is one of the types of *myrrh* which has been utilized in the treatment of twisted and as a fast-acting medicine (Alwhibi et al., 2020), likewise it is a powerful antimicrobial specialist as it is valuable for the treatment of skin breakout, bubbles, and joint pain. It shows solid antithrombotic activity (Bhattacharjee and Alenezi, 2020). *Myrrh* extract has been utilized as reducing (Elia et al., 2014) self-assembly (Zhao et al., 2018) and covering specialists (Atta et al., 2014) for the union of NPs which could be the benefit over microbial combination as there is no need of the explained course of refined and keeping up with the

phones (Wu et al., 2010). *Myrrh* has neighborhood energizer and insect mending, and disinfectant properties for wounds and scraped spots. It is utilized as a mouth wash (Eid et al., 2021), and as a uterine energizer and emmenagogue, it is utilized in the treatment of diseases in the mouth such as mouth ulcers, pyorrhea as well as catarrhal issues of pharyngitis and sinusitis. It is incredible in irritated mouth and outrageous ulceration of inconsistent ptyalism. The concentration of *myrrh* (gum) diminishes the outright augmentation of blood glucose over the fasting focus consistently of the oral glucose resistance test in both ordinary and diabetic rats (Al-Awadi and Gumaa, 1987), and may end up being a valuable helpful specialist in the treatment of non-insulin subordinate diabetes mellitus. A color of *myrrh* is utilized for the treatment of aphthous ulcers (stomatitis aphthosa). It shows solid antithrombotic movement. Extract of *myrrh* is utilized as stomach-related help medication, and it is endorsed by the FDA for the utilization in food and oral medical care drug items. It was given GRAS status as a flavor fixing by FEMA (Satpathy et al., 2020). *Myrrh* is utilized in conventional Chinese medication to diminish torment and enlarging because of awful injury (Lee and Lam, 1993). It is utilized as a hypolipidemic specialist. *Myrrh* is helpful in constant gastritis and nuclear dyspepsia with full pale tongue and layer, as well as successive mucous stouts joined by a fart. It helps in the treatment of laryngitis and respiratory whines. As of late the cytotoxic and antitumor movement of *myrrh* has ended up being identical to those of the standard cytotoxic medication cyclophosphamide. It likewise offered insurance against mucosal harm brought about by indomethacin (Al-Harbi et al., 1997). *Commiphora molmol* showed mitigating action, it showed an undeniable hindrance of ADP, adrenaline, and serotonin-instigated platelet collection. It additionally showed a solid thyroid stimulatory activity when directed to pale-skinned person rodents (Wijesekera, 2016). The constituents of *myrrh*, incorporate unpredictable oil (2–8%), tar (23–40%), gum (40–60%), and harsh standards (10–25%) (Chen et al., 2013). In Fig. 1 compound of *myrrh* incorporate phenols, furan sesquiterpenes, β -sitosterol, and liquor dissolvable tars with powerful sterile, cancer prevention agent and calming exercises which can be utilized actually in the mending of different kinds of wounds and ulcers (Cao et al., 2019; Negahdari et al., 2017; Walsh et al., 2010). The antimicrobial activity of phenolic compounds is portrayed by restricting nucleophilic amino acids in bacterial proteins, which prompts inactivation of the protein and loss of its capacity, in this way avoidance of the bacterial life cycle (Wink and Mitchell, 1998). Besides, phenolic intensifies focus on a superficial level of uncovered adhesins in the microbial cell, which will forestall bacterial adherence with different cells and arrangement of biofilms. In this concentration, it is zeroed in on the amalgamation of GNPs to raise the effectiveness of *myrrh*, and it is involved in the treatment of wound sterilization (Haffor, 2010), and come to an incredible outcome. In this methodology, the regular non-poisonous fixing removed from the *myrrh* plant was utilized, rather than normal unsafe synthetic compounds, in a blend with UV light illumination to synthesize GNPs. The *C.myrrh*@GNPs are homogenous, round, and three-sided shape, accomplish 1.68–10 nm particular sizes, and are all around scattered without collection, the portrayal of combined GNPs under various circumstances was dissected utilizing UV-apparent retention spectra, high-resolution transmission electron microscope (HR-TEM) examination, transmission electron microscope (TEM), fourier-transform infrared spectroscopy (FT-IR), powder XRD, dynamic light dissipating (DLS), energy dispersive X-ray spectroscopy (EDS), X-beam photoelectron spectroscopy (XPS) analysis and zeta potential.

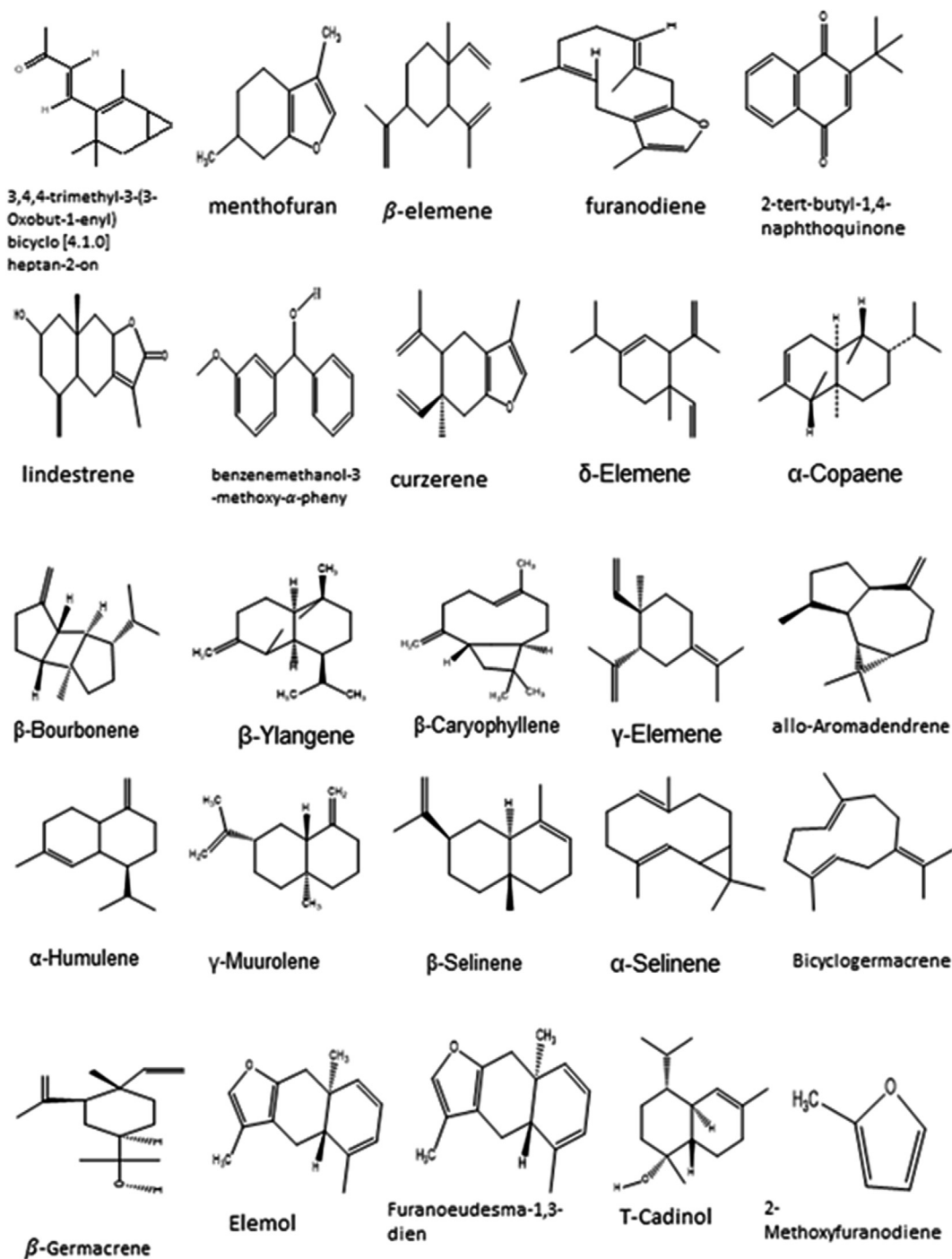


Fig. 1. Chemical structure of the main compounds polyphenols in *C.myrrh*.

This study investigated the property of *C.myrrh* extract in the development of GNPs and cell reinforcement, cytotoxicity, anticancer, mitigating, hostile to diabetic, and anti-microbial specialists. These amino acids and nutrients are likewise present in *C.myrrh* separate in the Kingdom of Saudi Arabia (KSA) locale. The current article investigates the natural potential of the antioxidants, amino acids and some secondary metabolites of a particular *C.myrrh* plant for the biosynthesis of GNPs. The biosynthesized *C.myrrh*@GNP applied as a multi pharmaceutical agent including anti-diabetic, antibiotic, anti-oxidant, antibacterial, anti-inflammatory and lastly anti tumorigenic towards two malignant growth cell lines, colon carcinoma (HCT-116) and breast adenocarcinoma (MCF-7).

2. Materials and methods

2.1. *C.myrrh* extract preparation

The oleo-gum-resin of *C.myrrh* was bought from a local market in Madinah Munawara, KSA, and washed with double distilled water (ddH₂O) followed by ethanol. The oleo-gum-resin of *C.myrrh* was grounded into coarse powder by a grinder. The oleo-gum-resin of *C.myrrh* powder (500 mg) was extracted using ethanol or ddH₂O by maceration for 24 h (h) at room temperature (RT) with occasional shaking (250 g × 2L). The extract was then filtered and dried by rotatory evaporator. The oleo-gum-resin of *C.myrrh* extract was utilized for further experiments.

2.2. Synthesis of GNPs

(HAuCl₄ · 3 H₂O) derived from Sigma Aldrich with high purity (9.99%), *C.myrrh* stock solution prepared and mixed with 4 ml volume of (1 × 10⁻³) M of HAuCl₄ · 3 H₂O. The reduction reaction of Au⁺³ to Au⁰ was confirmed when the yellow color changed to ruby-red.

2.2.1. Optimization for *C. myrrh*@GNPs synthesis

A few elements influence the combination of GNPs, for example, the amount of *myrrh* extract, the amount of (HAuCl₄ · 3 H₂O), response time, pH, and the temperature was contemplated to gauge the improvement boundaries for the union of *C.myrrh*@GNPs from an extract of *myrrh*.

2.2.2. Optimization for *C. Myrrh* extract

Various volumes of *C. myrrh* extract from 1 to 6 ml were treated with 4 ml of 1 mM HAuCl₄ · 3 H₂O independently and the temperature was retained at RT intended for around 80 min for the production of *C.myrrh*@GNPs.

2.2.3. Optimization for the volume of HAuCl₄ · 3 H₂O

The impact of volume of HAuCl₄ · 3 H₂O to 6 ml of *C.myrrh* extract was examined by treating 1 to 4 ml volumes of HAuCl₄ · 3 H₂O. independently for about 80 min at RT.

2.2.4. Optimization for the reduction of time

The reaction response time impact was examined by checking the UV-Vis spectra of *C.myrrh*@GNPs synthesized in the solution having maintained reaction time from 20 to 120 min, and different volumes of *C.myrrh* extract and gold salt.

2.2.5. Optimization of pH

A pH optimization was studied at various levels from 1 to 9 after 80 min of reaction time with optimized *C.myrrh* extract and salt concentration at RT. The optimization study of pH was done by 0.1 M HCl and 0.1 M NaOH.

2.2.6. Optimization for reaction temperature

The reaction temperature was examined by setting different reaction temperatures from 15 °C to 35 °C for around 80 min with the above-streamlined conditions to acquire *C.myrrh*@GNPs.

2.3. Characterization of GNPs

To guarantee the physio-substance nature of incorporated *C. myrrh*@GNPs, an assortment of insightful methods were utilized for the investigation. UV-Vis absorbance spectra were done with quartz cuvettes utilizing Cary 100, UV-Vis spectrophotometer within the frequency range 200–800 nm wavelength. FTIR was achieved upon Thermo Nico-let 6700 within the 200–4000 cm⁻¹ range to analyze the presence of possible functional groups. The crystalline nature of *C.myrrh*@GNP was studied by powder XRD using Shimadzu XRD-7000, Japan. The size and the surface morphology of *C.myrrh*@GNPs were inspected via TEM examination done upon JEOL/JEM2100, at 90 KV and utilizing HR-TEM. The existence of the gold component and other components was affirmed using EDX examination utilizing a JEOL EDX, JSM-5610 LV model. Dynamic light scattering (DLS) is a significant method moderately used to understand the distribution of the size of tiny particle that exists within a solution. The light dissipating strategy was used to concentrate on the genuine size circulation profile of *C.myrrh* mediated produced GNPs. For the X-ray photoelectron spectroscopy (XPS) study, a

Physical Electronics PHI 5000 Versa test II instrument was utilized.

2.4. Antioxidant study

Antioxidant study of HAuCl₄ · 3 H₂O, *C.myrrh* and *C.myrrh*@GNP entirely set in stone by (Al-Radadi, 2021b; Hosseinimehr et al., 2011), where 50 µL of various convergences of HAuCl₄ · 3 H₂O, *C.myrrh* and *C.myrrh*@GNPs were occupied in various test tubes, then, 2.5 ml of 0.1 mM DPPH methanolic arrangement was mixed with these test tubes and thoroughly shaken. The test tubes were permitted to remain at 25 °C for 20 min. The separate control test tube was made ready as above utilizing methanol dissolvable rather than HAuCl₄ · 3 H₂O, *C.myrrh* and *C.myrrh*@GNPs. The DPPH free radical scavenging test was completed for the assessment of the antioxidant test. This examines the free radical scavenging limit of the researched extricate. DPPH is a particle including a steady free extremist. Within the sight of a cell reinforcement, which can give an electron to DPPH, the purple tone commonplace for nothing DPPH radical rots, and the alteration in absorbance is estimated at λ = 517 nm. The anti-radical action of the GNPs, *C.myrrh*, and *C.myrrh*@GNPs was estimated as the free extremist rummaging action DPPH. Shortly, within 3 ml of every GNPs, *C.myrrh*, and *C.myrrh*@GNPs 1 ml of methanol arrangement of 0.1 mM/L DPPH solution was mixed. The combination was set aside in dark RT intended for 30 min and the absorbance was estimated at λ = 517 nm against a blank. The percentage activity of free radical scavenging was determined utilizing the following formula:

$$\% \text{ potential of DPPH free radical scavenging} = \frac{(\text{control-test})}{\text{control}} \times 100.$$

IC₅₀ upsides of the HAuCl₄ · 3 H₂O, *C.myrrh* and *C.myrrh*@GNPs, for example, the convergence of HAuCl₄ · 3 H₂O, *C.myrrh* separate and *C.myrrh*@GNPs. Important to diminish the underlying union of DPPH by half were determined. The IC₅₀ esteem µg/ml is the viable focus at which DPPH radical was looking through by half and the worth was acquired by addition from the straight declined examination.

2.5. Examination of cell viability against of *C.myrrh* extract and *C. myrrh*@GNPs

For cell viability study, Human umbilical vein endothelial cells (HUVECs) were cultivated in M199, enhanced with heat-inactivated 20% FBS (WELGEN Inc.), 20 ng/ml of bFGF, 100 units/ml of penicillin, and 100 µg/ml of streptomycin within 5% CO₂ incubator at 37 °C.

The impact of HAuCl₄ · 3 H₂O, *C.myrrh*, and *C.myrrh*@GNPs on the suitability of HUVECs were resolved to utilize the MTT (3-(4,5-dimethylthiazol-2-yl)-2,5-diphenyl tetrazolium bromide) test, which depends on the change of MTT to insoluble MTT-formazan by cleavage of the tetrazolium ring by mitochondrial dehydrogenase compounds in living cells (Al-Radadi, 2022a; Arulmozhi et al., 2013). In brief, HUVECs were developed in M199 with 20% FBS at a thickness of 2 × 10⁴ cells on 24-well culture plates. Following one night, the media was supplanted by M199 including 1% FBS, and HAuCl₄ · 3 H₂O, *C.myrrh*, and *C.myrrh*@GNPs and the cells were then brooded for 24 h at 37 °C under a humidified air that included 5% CO₂. The cells were allowed to react with different concentrations of HAuCl₄ · 3 H₂O, *C.myrrh*, and *C.myrrh*@GNPs. Then, 5 mg/ml in H₂O of MTT solution was added to each well, trailed by the addition of 0.3 ml of dimethyl sulfoxide to break down the MTT-formazan. MTT formazan was estimated by recording the optical density at 570 nm wavelength as indicated by the

following equation. The experiment was performed in triplicate and repeated thrice.

$$\text{Percentage of cell viability (\%)} = \left(\frac{\text{Sample Absorbance}}{\text{Control Absorbance}} \right) \times 100$$

2.6. Cytotoxicity activity

MTT compound was used to assess cell toxicity (Al-Radadi, 2022c, 2021a; Yas et al., 2021). Cell lines of the colon (HCT-116) and breast carcinoma (MCF-7) were grown in Eagle's minimum essential medium with 2 mM L-glutamine concentration and Earle's salts. In a nutshell, the cell lines were allowed to grow at 1×10^4 cells/well in a 96 well plate, then incubated at 37 °C in a 5 percent CO₂ incubator for 24 h. *C.myrrh* and *C.myrrh*@GNPs were used in concentrations of 15 g, 25 g, 50 g, and 100 g and incubated for 24 h. Following a 4 h incubation period, MTT (5 mg/ml in PBS) was added to each well. After discarding the supernatant, 100 μL of DMSO was mixed in each well of the plate, which was then smoothly shaken for dissolving the formazan formed and recorded the absorbance utilizing a plate reader at 530 nm. The inhibition of cell growth in percentage was measured utilizing the following formula and the concentration required for inhibiting 50% of the cell growth was also assessed for *C.myrrh* and *C.myrrh*@GNPs. DMSO was selected as negative control while doxorubicin was added as a standard drug and acted as a positive control.

The IC₅₀ standards were estimated by mean values of three experiments with four concentrations.

$$\% \text{ Inhibition} = 100 - \left(\frac{\text{OD of Sample}}{\text{OD of Control}} \right) \times 100$$

2.7. Anti-inflammatory assay

Cyclooxygenase (COX) is an enzyme that produces prostaglandins that cause fever, pain, and inflammation. Herein, the biosynthetic GNP was examined for inhibition potential to COX-1 and COX-2 enzymes to decrease inflammation. COX-1 and COX-2 from Ovine Kit 701050, France were used to measure the anti-

inflammatory capacity of *C.myrrh*@GNP. For positive control ibuprofen (10 mM) was utilized. NPs of various concentrations, including 25, 50, 100, 200, and 400 μg/ml were utilized for test inhibition and calculated according to the manufacturer's instructions. 96-well microplates were scanned at 530 nm wavelength absorbance for the presence of N, N, N', N' tetramethyl-p-phenylenediamine.

2.8. Antidiabetic assay

An *α*-amylase and *α*-glucosidase assays were performed to evaluate the anti-diabetic potential.

2.8.1. *α*-amylase

The capacity of concentrates to repress *α*-amylase was examined utilizing a chromogenic technique recently depicted by (Sigma Aldrich, USA). In 0.1 M phosphate buffer having pH 6.8, the 1 m/ml protein was ready and completely blended in with 5 mM, 4-nitrophenyl-*α*-D-maltopentaoside solution. A little part of the examination sample was acquainted with the reaction mixture and incubated for 30 min at 37 °C. The percent inhibition activity of the sample was determined by subtracting the absorbance of two samples when the reaction mixture include extract and while it was excluded by utilizing a microplate reader at wavelength 530 nm.

2.8.2. *α*-glucosidase

To further evaluate the anti-diabetic potential, the *α*-glucosidase inhibition test was carried out using a color-producing method having a 0.45 m polyethylene filter end-capped column. A little portion of the experimental sample was reacted with 5 mM of 4-nitrophenyl-D-glucopyranoside (4NPG; Sigma, country name?) 1 ml of intestinal fluid and allowed to incubate at 37 °C for 30 min. The potential activity was evaluated using percent inhibition potential via calculating a diversity between absorbance standards while containing the extracts and the absorbance of the examined sample on a 530 nm wavelength.

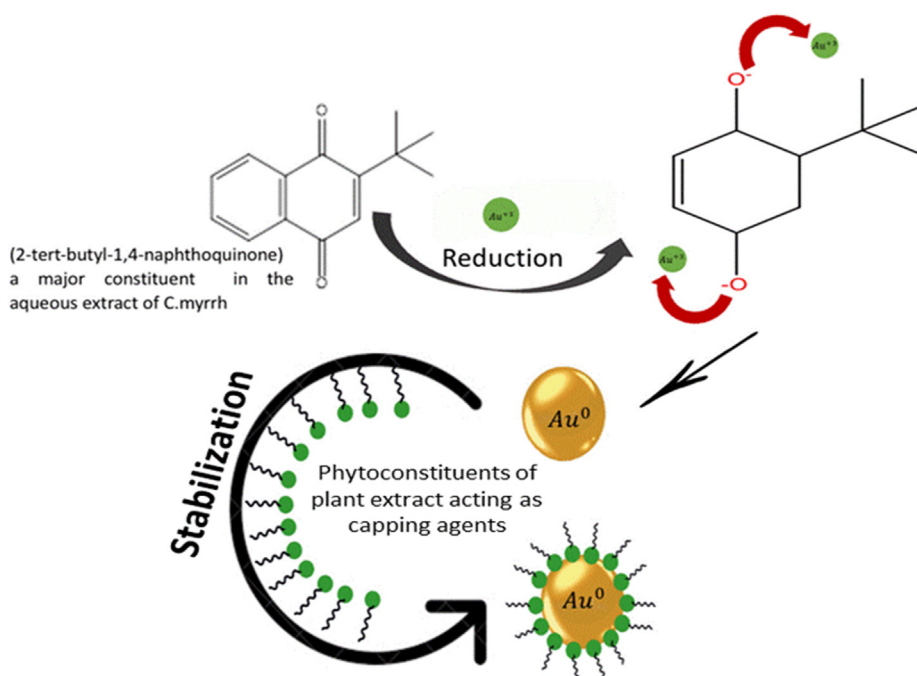


Fig. 2. Schematic diagram for the reduction process and stabilization of GNPs by *C.myrrh* aquas extract, the work plane for synthesis of *C.myrrh*@GNPs.

2.9. Bioassay of antibacterial activities

The antibacterial effectiveness of every extract was tested utilizing a total of four bacterial strains, two of which were *Staphylococcus aureus* and *Bacillus subtilis* Gram-positive and two of which were *Escherichia coli* and *Pseudomonas aeruginosa*, Gram-negative that contaminate food. The strains of bacteria were derived from King Fahad Medical Research Centre (KFMRC) at King Abdulaziz University, Jeddah, Saudi Arabia.

2.9.1. Agar well diffusion method

The anti-bacterial potential of *C.myrrh*@GNPs was analyzed using the conventional agar well diffusion technique (Kunchandy and Rao, 1990) utilizing a 5 mm borer about six wells were created in an aseptic environment. The bacterial cultures were poured throughout the Petri plates by spreader and various *C.myrrh* extract concentrations and *C.myrrh*@GNPs were added to 15 µg/ml, 25 µg/ml, 50 µg/ml, and 100 µg/ml, into the 5 mm well. Streptomycin acted as a positive control and lacking samples were retained as a negative control. The Petri plates were kept at 37 °C for incubation for 24 h. The inhibition area was calculated by a MIC ruler along with mentioned in mm.

2.10. Molecular docking

2.10.1. Preparation of ligand

The main compounds polyphenols in *C.myrrh* planned to be used for docking were prepared using the default protocol of the Ligprep program (2021) in the Schrodinger's suite. All compounds were docked to the target protein using the glide dock XP protocol without using perform post-docking minimization. XP G-score (Kcal mol⁻¹) was used as ranking criteria for the best-docked ligands.

2.10.1.1. Preparation of protein. VEGFR-2 was found to be crucial for cell survival, which regulates endothelial differentiation in both

the breast cancer cells (MCF-7) and human colorectal carcinoma (HCT-116) (El-Adl et al., 2021). Thus each experiment used VEGFR-2 downloaded from the Protein Data Bank (PDB ID: 1YWN) (Miyazaki et al., 2005). Furthermore, the three-dimensional structures of ovine COX-1 (PDB ID: 3KK6) (Rimon et al., 2010) and mouse COX-2 (PDB ID: 3LN1) (Wang et al., 2010) were selected for anti-inflammatory docking (Karim et al., 2019). Finally, for the antidiabetic docking (Missioui et al., 2021), the crystal structure of α -amylase (PDB ID: 4GQR) (Williams et al., 2012) and α -glucosidase (PDB ID: 5NN5) (Roig-Zamboni et al., 2017) were selected.

All three-dimensional complex structures were downloaded from the PDB database (<https://www.rcsb.org/>). The protein structures were prepared using the protein preparation wizard program from the Schrödinger suite (Schrödinger Suite, 2021-2) in which water molecules (>5Å radius) and small molecules present were removed from the structure part, disulfide bonds were created and hydrogens were added to the PDB structures. Restrained imperf minimization with default settings was performed on the structure with optimized potentials for liquid simulations (OPLS-2005) force field. The resulting structures were used for receptor grid generation for docking.

3. Result

3.1. Analytical study of *C.myrrh*

GNPs were synthesized in a green, environmental technique with an eco-friendly approach without using any organic solvent. Several devices were used to characterize GNPs synthesized with *myrrh* extract, under several conditions of reaction, the production of GNPs was performed within the different environments including at various temperatures, pH, varying time intervals varying volumes of *C.myrrh* extract, and gold salt. From experience, it is found that the best result to get the best images taken by electron microscopy of GNPs were observed to be small, spherical, homogeneous,

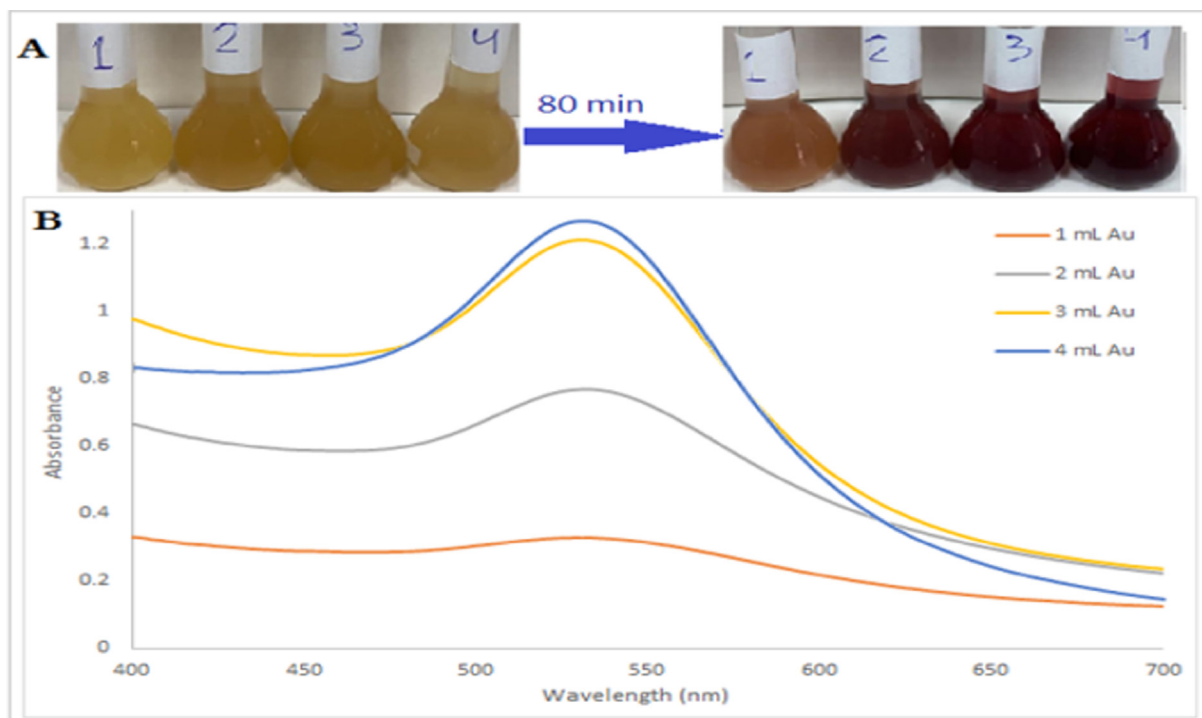


Fig. 3. UV-Vis spectra of *C.myrrh*@GNPs at different volumes of (1–4 ml) (HAuCl₄·3H₂O) (1 × 10⁻³)M with (6 ml) of *C. myrrh* extract at room temperature 25 °C after 80 min.

and with no aggregation, when *C.myrrh* extract (6 ml) was added to 1 mM $\text{HAuCl}_4 \cdot 3\text{H}_2\text{O}$ (4 ml) and after 80 min at 25 °C and pH 4.5. The solution color transformed to ruby-red from yellow. Studying the UV–VIS spectroscopy of *C.myrrh*@GNPs showed various absorbance peaks, it is found that the surface plasma resonance (SPR) for GNPs strong, and the best peak for the highest absorption $\lambda_{\text{max}} = 532\text{nm}$. It is noticed that in Fig. 3 small amount of volume, the absorption is too low and broad, but when the increase the volume, the absorption increases as it becomes sharper and narrower, the best volume was (6 ml) absorbed at 1.4 and $\lambda_{\text{max}} = 532\text{nm}$ in Fig. 4. It is noticed that when the volume of $\text{HAuCl}_4 \cdot 3\text{H}_2\text{O}$ increased the absorption increased as well, the best curve observed for 4 ml at wavelength 532 nm as shown in Fig. 4. It can be seen that (4 ml) of ($\text{HAuCl}_4 \cdot 3\text{H}_2\text{O}$) is narrower and sharper than (3 ml) which is broad which indicates the formation of GNPs. In Fig. 5, the time effect on *C.myrrh*@GNPs can be seen with the best absorption at 80 min, when GNPs form at a wavelength $\lambda_{\text{max}} = 532\text{nm}$ and absorption more than 2. Fig. 6. strength variations of UV–Vis peak of GNP as a purpose of (4 ml) ($\text{HAuCl}_4 \cdot 3\text{H}_2\text{O}$) and (6 ml) of *C.myrrh* extract following 80 min after mixture at 25 °C. The absorbance spectra present at 532 nm corresponds to Au^0 that showed continuous increase till 80 min. and stabilized at a 532 nm peak that is equivalent to the synthesis of Au^0 nanostructures. There was a difference in UV Vis absorbance spectra and time is taken to achieve stabilized λ_{max} demonstrated by absorbance to time spectra. These findings recommended that the first 80 min is sufficient to accomplish the uppermost concentration of stabilized *C.myrrh*@GNPs. Fig. 7 showed the best effect of temperature on GNPs at 25 °C that

have absorption at 1.9 and wavelength $\lambda_{\text{max}} = 532\text{nm}$, which was the narrower and sharper at pH 4.5. It is noticed that the best absorption with wavelength $\lambda_{\text{max}} = 532\text{nm}$ then the absorption decreases every time increased the pH which is shown in Fig. 8.

3.2. TEM analysis

With the aim of the morphological and size-dependent study of the *C.myrrh*@GNPs electron microscopy was performed in transmission mode. The size of *C.myrrh*@GNPs found in TEM images ranges from 1.68 – 7.86 nm. The TEM images of *C.myrrh*@GNP in Fig. 9-B presented nano size with spherical shape and did not exhibit aggregation. Further approach devoted to morphological study shown in TEM images (Fig. 9-A) given a clear idea of the size of *C.myrrh*@GNPs range from 1.68 nm, 7.86 nm, and 10.8 nm at 20 nm resolution. The HAADF-STEM images of the *C.myrrh*@GNPs in (Fig. 9-C) demonstrate the gold in bright ring structures. Additionally, the intensity of 4 nm diameter-sized nanoparticles was confirmed in the Fig. 9-D.

3.3. EDX study

Further characterization of the elemental gold was performed by the EDX technique. The elemental analysis profile of *C.myrrh*@GNPs exposed a sturdy signal for gold at 2.8 KeV alongside carbon and oxygen peaks. The consequential other signals may arise due to the secondary metabolite capped around the surface of the *C.myrrh*@GNPs (Fig. 10).

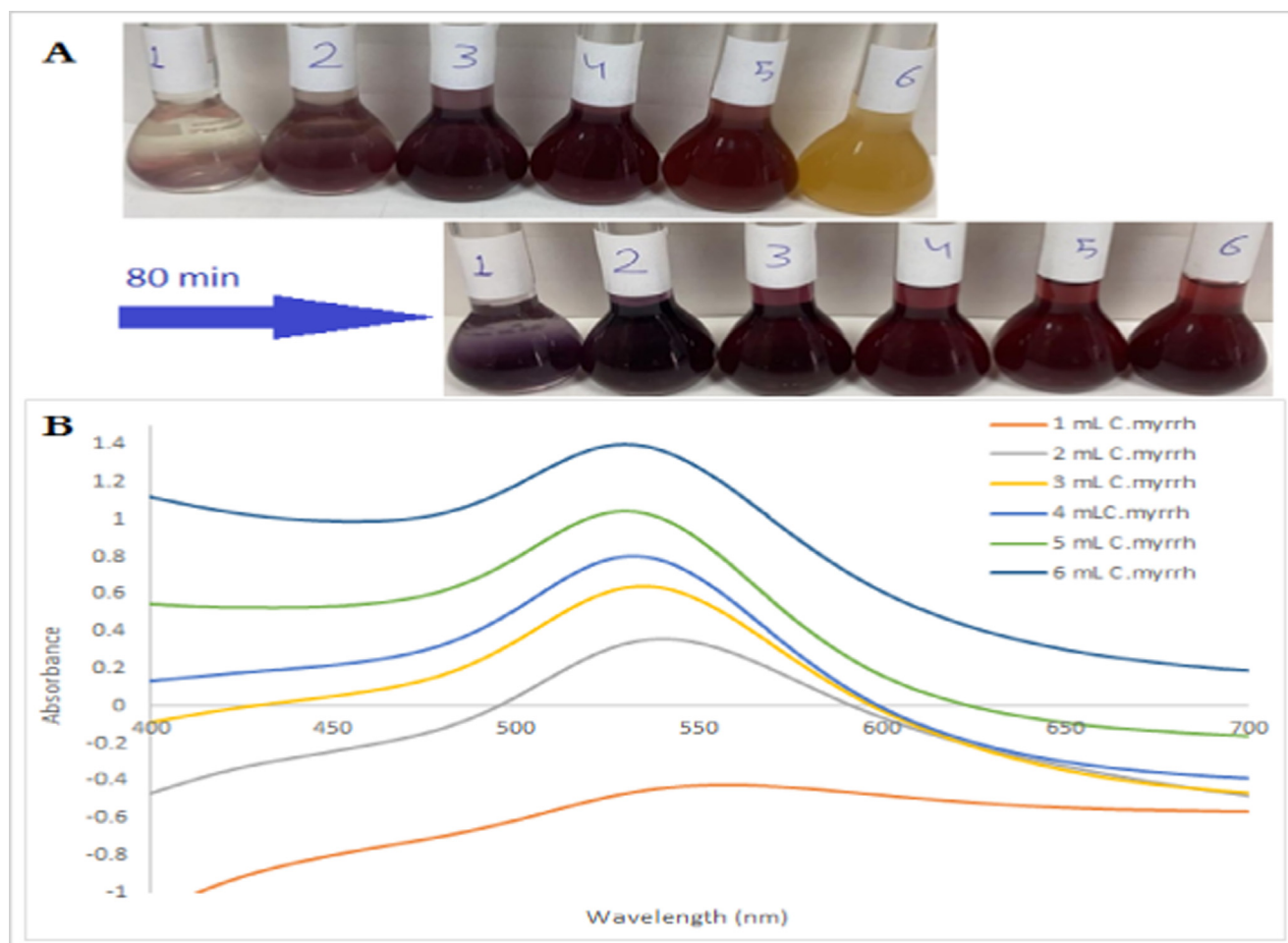


Fig. 4. UV–Vis spectra of *C.myrrh*@GNPs at different volumes of *C. myrrh* extract (1–6 ml) with (4 ml) ($\text{HAuCl}_4 \cdot 3\text{H}_2\text{O}$) ($1 \times 10^{-3}\text{M}$) after 80 min at room temperature 25 °C.

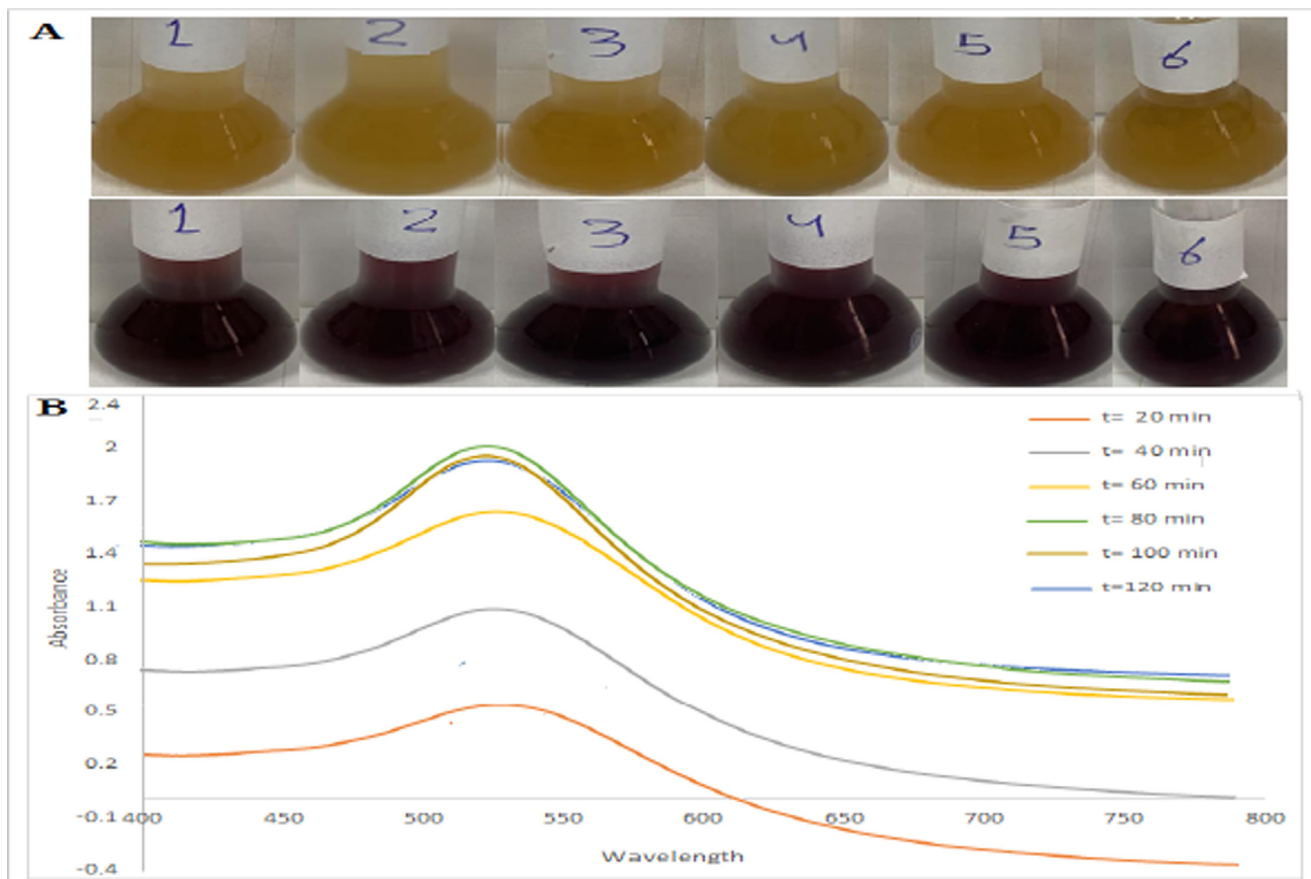


Fig. 5. Intensity variant within UV-Vis. spectra of *C.myrrh*@GNPs as function of time at room temperature 25 °C with (6 ml) of *C.myrrh* extract and (4 ml) (HAuCl₄·3H₂O) (1 × 10⁻³)M.

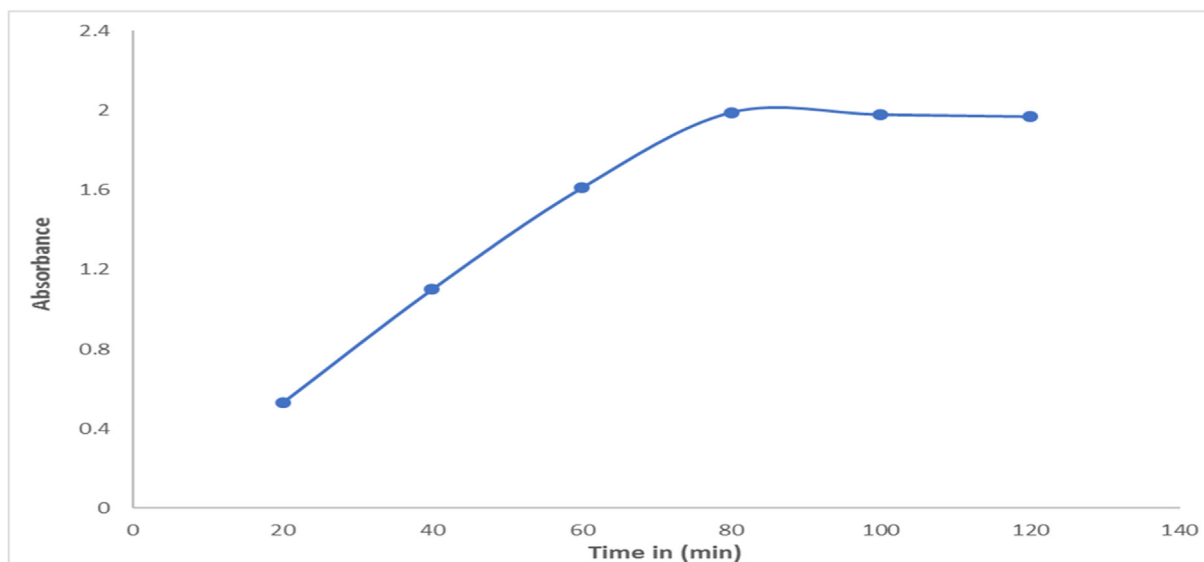


Fig. 6. Absorption Intensity variant within UV-Vis spectra of *C.myrrh*@GNPs as a function of (4 ml) (HAuCl₄·3H₂O) (110⁻³) M stock solution and (6 ml) of *C.myrrh* extract after 80 min of addition at 25 °C.

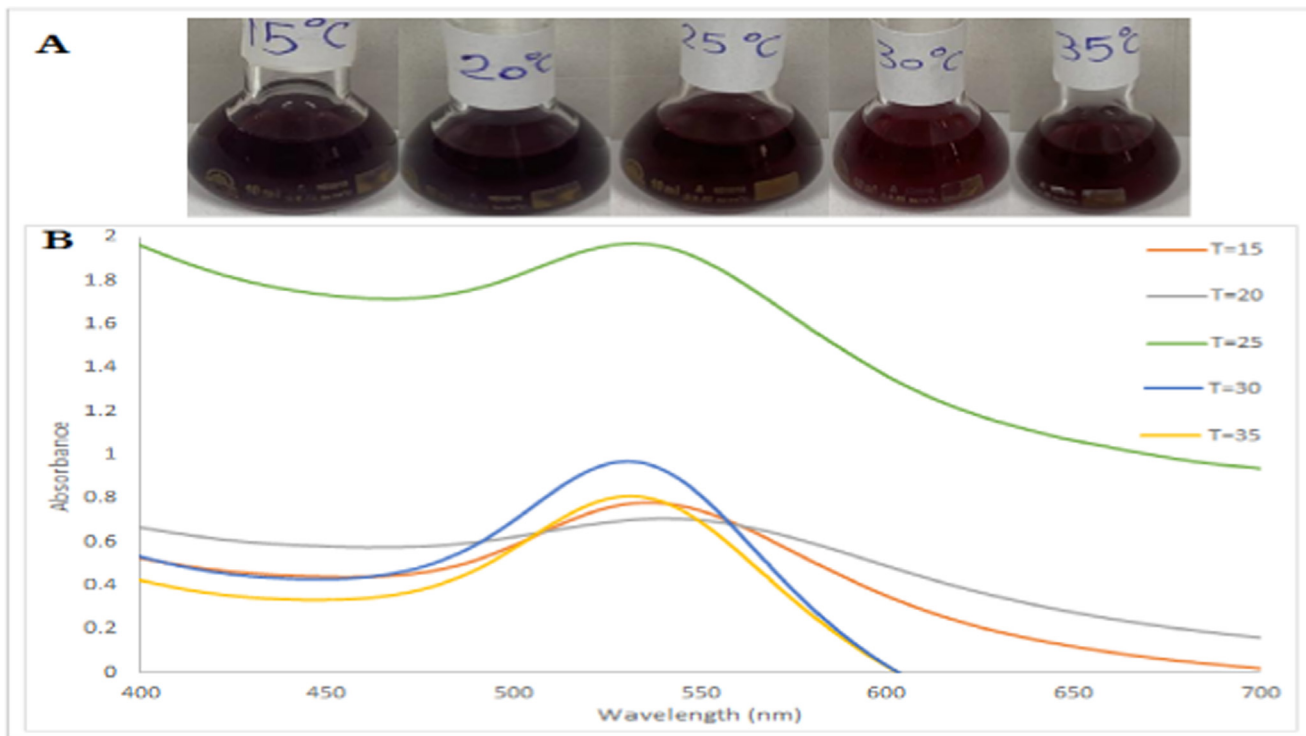


Fig. 7. UV-vis spectra for *C.myrrh*@GNPs at different temperatures (15–35), after 80 min with (6 ml) of *C. myrrh* extract and (4 ml) (HAuCl₄·3H₂O) (1×10⁻³) M.

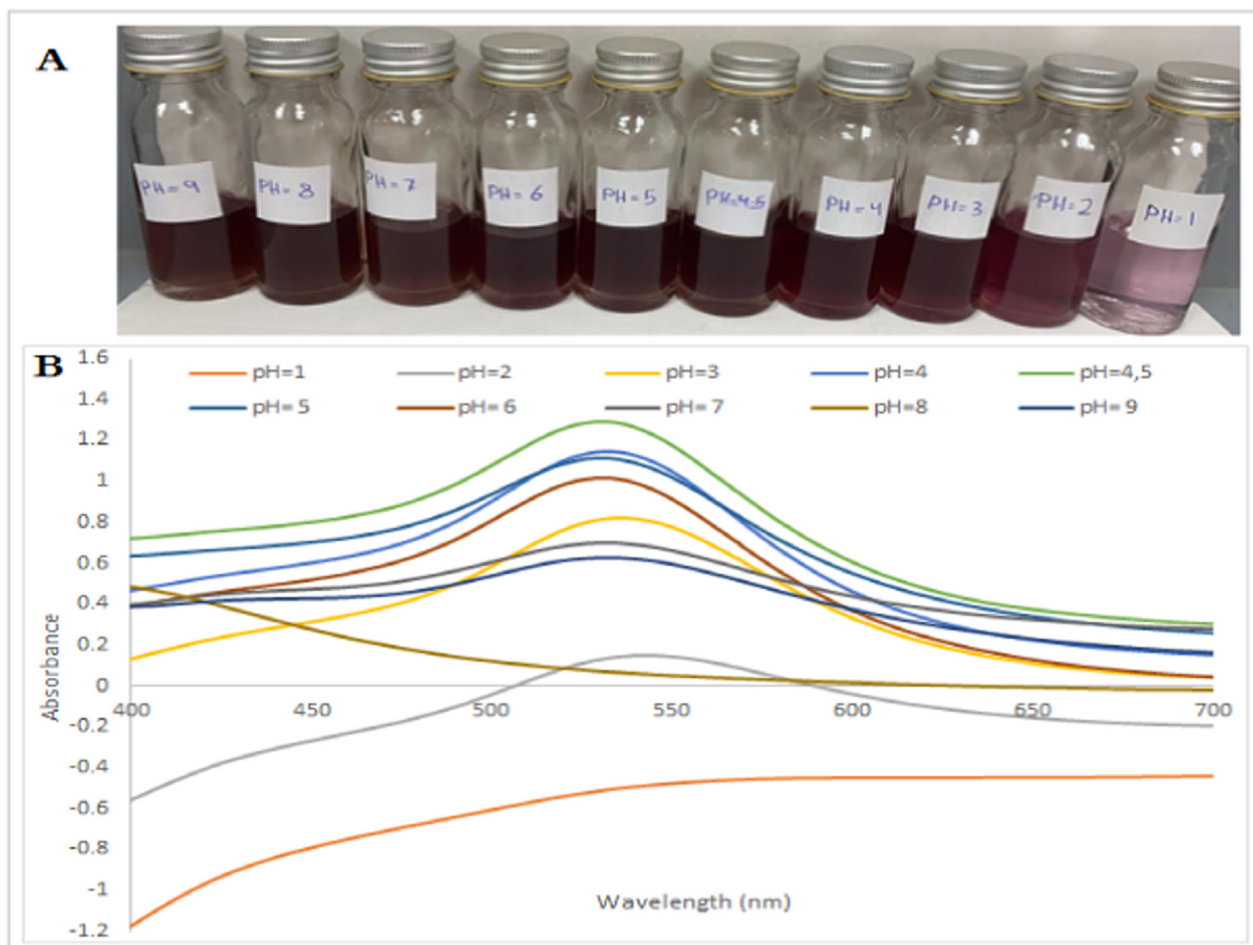


Fig. 8. UV-vis spectra for *C.myrrh*@GNPs at different pH values (1–9) at room temperature 25 °C, after 80 min with (6 ml) of *C.myrrh* extract and (4 ml) (HAuCl₄·3H₂O) (1×10⁻³) M.

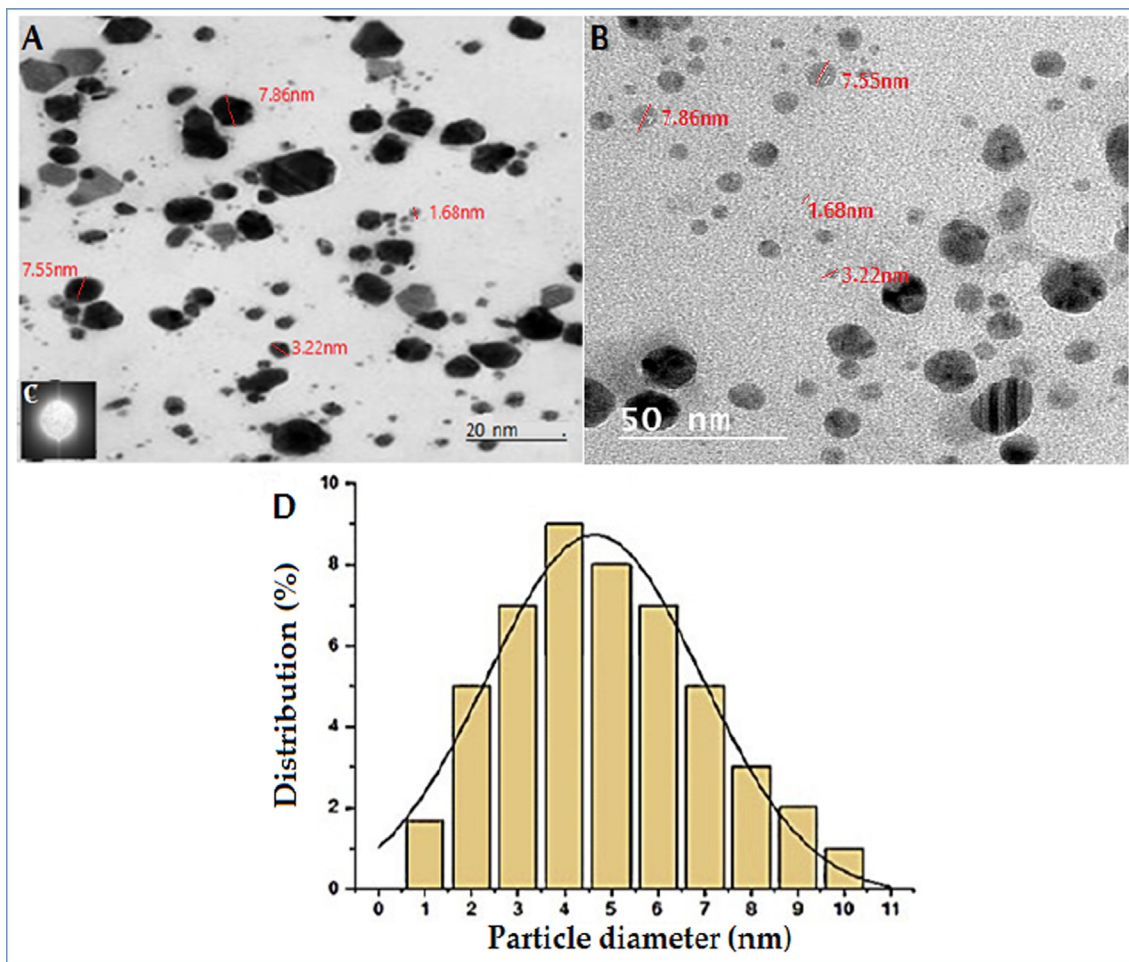


Fig. 9. (A) HR-TEM image of spherical C.myrrh@GNPs, (B) TEM image of C.myrrh@GNPs, (C) HAADF-STEM images of the C.myrrh@GNPs and the elemental mapping images, (D) Size distributions graph and of C.myrrh@GNPs.

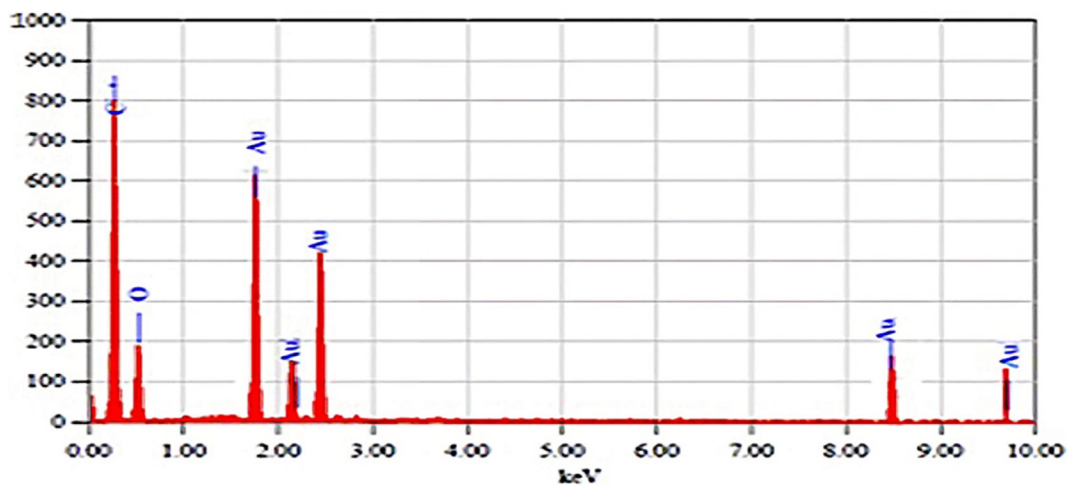


Fig. 10. EDX analysis for C.myrrh@GNPs.

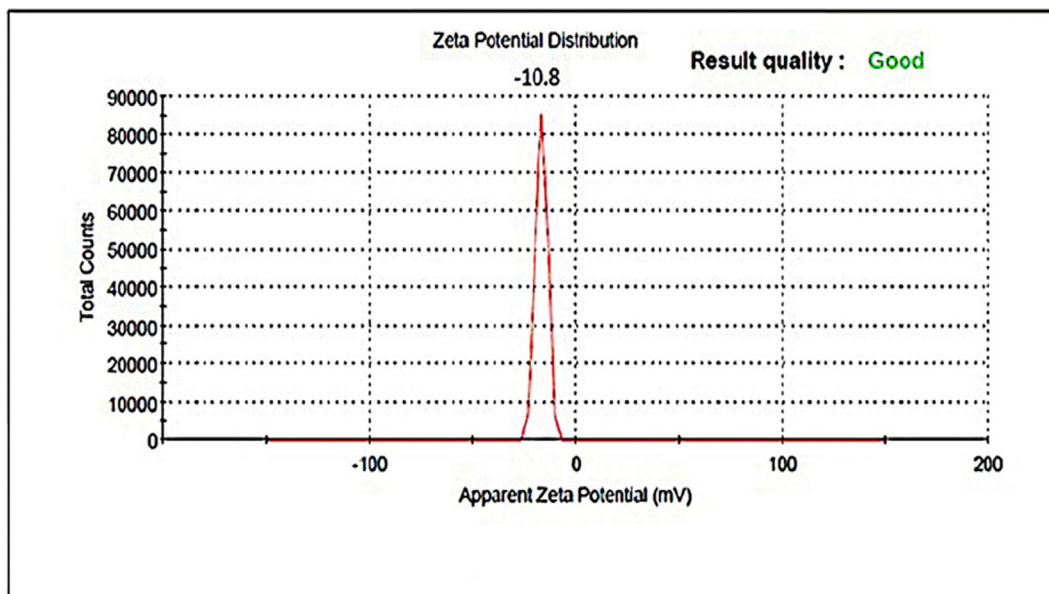


Fig. 11. Zeta potential of GNPs synthesized by *C.myrrh*.

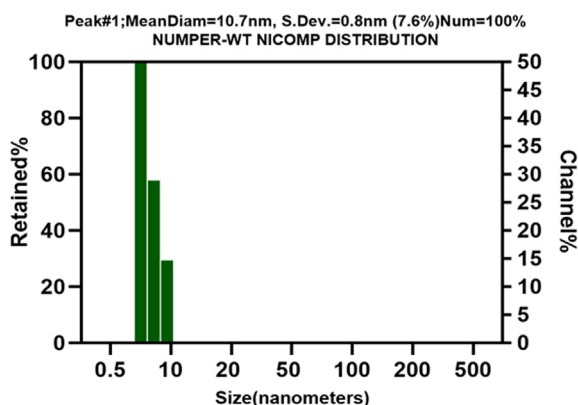


Fig. 12. DLS Size Distribution of GNPs synthesized by *C.myrrh*.

3.4. DLS analysis

The analysis of the zeta potential study found (-10.8) mV that indicated the stability of *C.myrrh*@GNPs at 25 °C (Fig. 11). It was in collaboration with the earlier images shown in TEM mean triplicate (Fig. 12).

3.5. FTIR analysis

FTIR analysis was completed to distinguish the bound bio-particles responsible for covering and producing GNPs utilizing *C.myrrh* extract (Fig. 13). The FTIR range of GNPs showed an exceptionally solid top at 3400 cm^{-1} was allocated as (-OH) bunches extending, the 3010 cm^{-1} peak acquired because of aromatic (C-H) bonds, where at 2900 cm^{-1} the top for aliphatic (C-H) gatherings, at 1700 cm^{-1} , wave-numbers tops happened because of the presence of (C=O) (carbonyl groups) and 1030 cm^{-1} (C-O) extending vibrations of alcohols, carboxylic acids, ester, or ethers of bio-particles present in the *C.myrrh*.

3.6. XRD study

XRD is an effective technique for analyzing crystalline materials, where it gives information about crystal structure and crystal size for Nanomaterial. X-ray diffraction of *C.myrrh*@GNPs showed 5 peaks at the range which is attributed to the sides of the cube are centered on the side of the crystal that applies to the Joint Committee for Powder Diffraction Set (JCPDS) with the known information of X-Ray diffraction for the gold metal. The crystalline character of *C.myrrh*@GNPs was examined using the X-Ray diffraction method and found four major peaks at 38.1, 44.5, 65, 78, and 82 coupled theta, allocated to (111), (200), (220), (311) and (222) crystalline planes respectively of gold. These found indices indicate the FCC structure of GNPs. In Fig. 14 the additional peak shown at 82 coupled theta may arise due to the extract's amorphous nature. The average crystallite size is determined by using the Debye–Sheerer formula: $D = \frac{k\lambda}{\beta \cos 2\theta}$

Where D represents the average thickness of crystalline grains, K represents the Scherrer constant (0.89), β represents the FWHM (Full-Width Half Maximum), θ represents the angle of diffraction, and λ represents the X-ray wavelength.

3.7. XPS analysis

To additionally affirm the existence of polyphenol covering the surface of the NPs, an XPS investigation was carried out. Fig. 15-A, demonstrate the settled spectra of the center degrees of Au4f_{7/2} and Au4f_{5/2} at 84 eV and 88 eV, separately, relating admirably with the earlier reports of metallic Au⁰. Fig. 15-B-C-D addresses the acquired spectra for N1s, C1s, and O1s, individually. The C 1s top at 284.5 eV and O1s top at 532.3 eV N1s top at 399.5 eV may be because of the extract of *C.myrrh*.

3.8. Antioxidant activity of GNPs by DPPH

DPPH (1,1-diphenyl –2-picryl-hydrazine) is a well-acknowledged approach to determining antioxidant characteristics as a result of its capacity in reducing the free radicals. DPPH radicals can

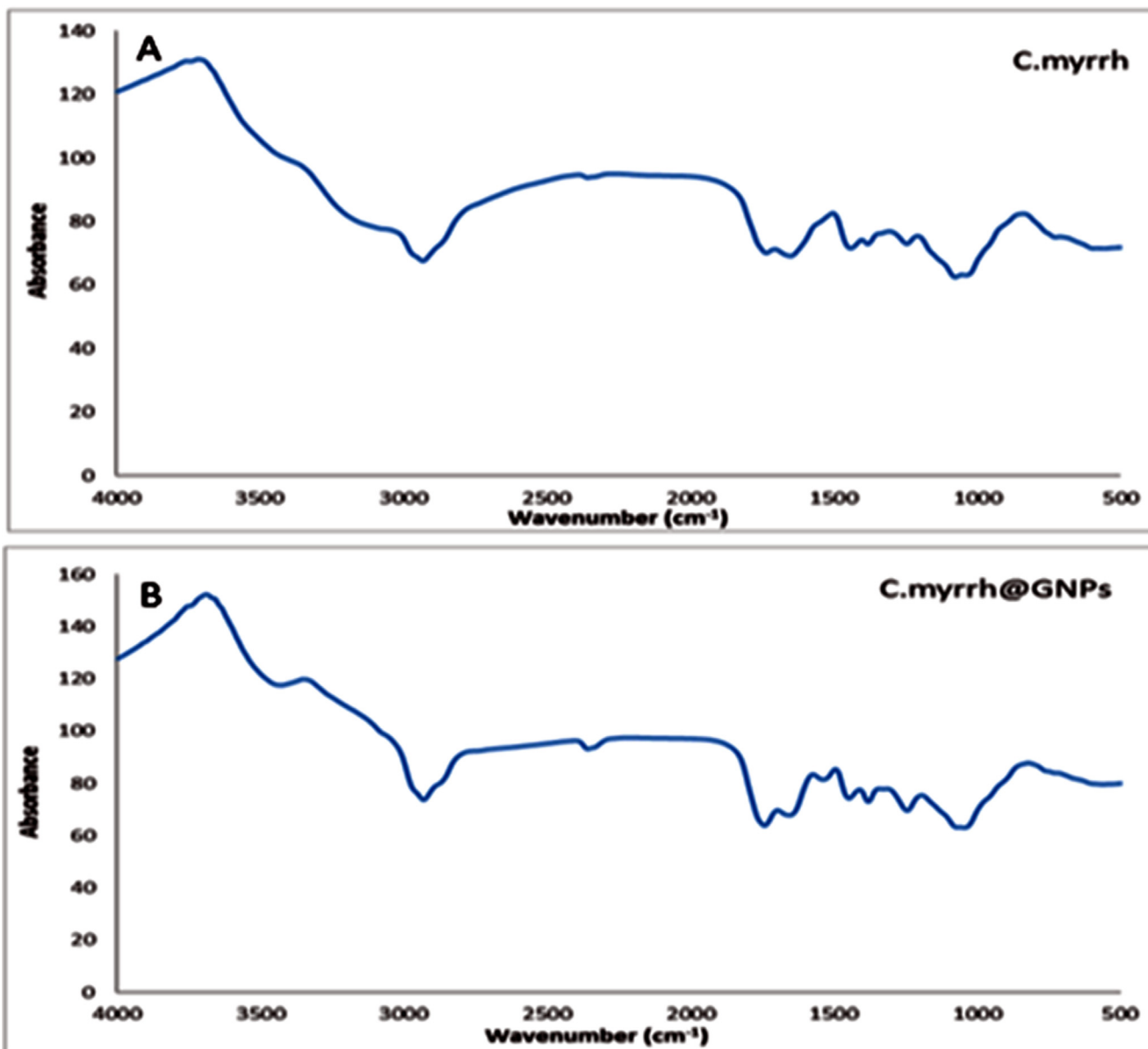


Fig. 13. FTIR spectrum of *C. myrrh* extracts and *C. myrrh*@GNPs.

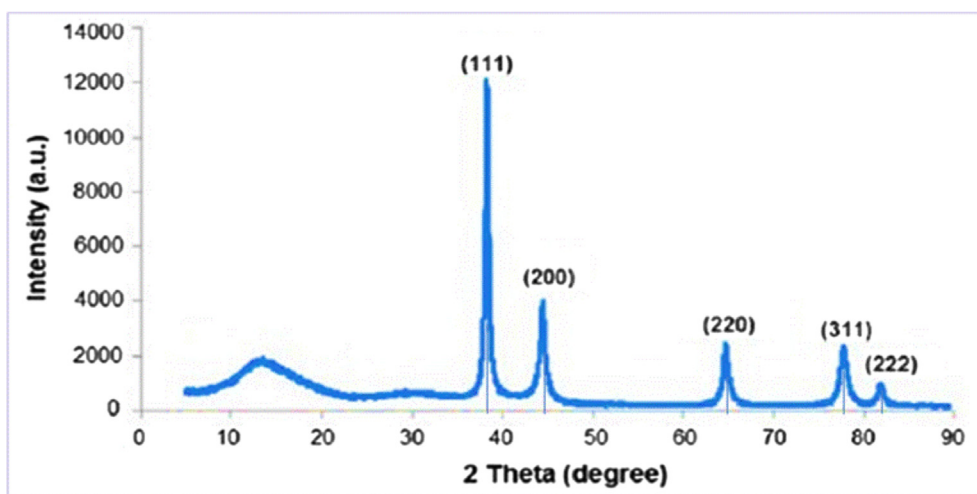


Fig. 14. XRD spectrum of synthesized GNPs with *C. myrrh* extract.

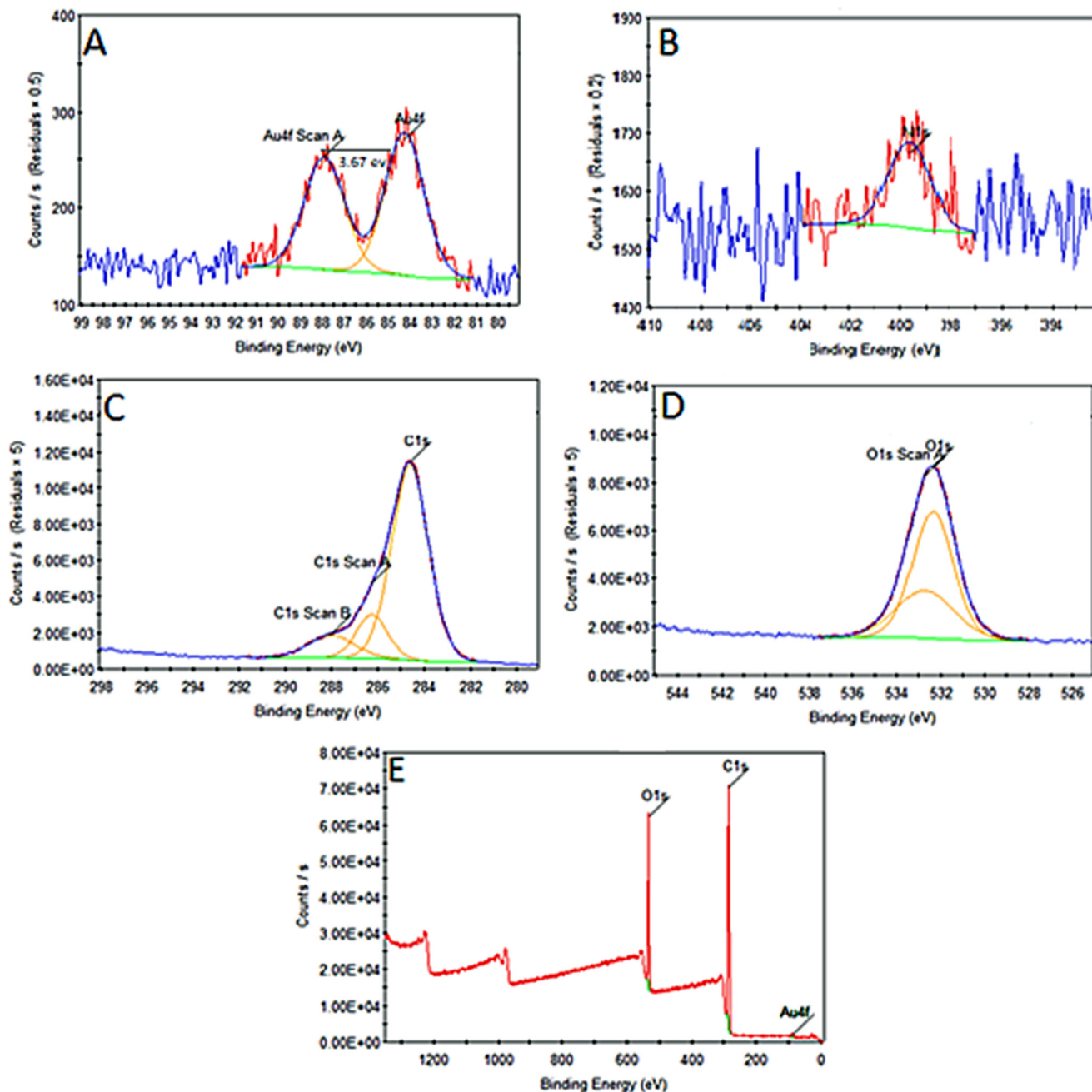


Fig. 15. XPS analysis showing survey scan (a) Au, (b) Nitrogen, (c) carbon and (d) oxygen, (E)survey.

immediately react to antioxidants. When antioxidants attract this radical, DPPH is revitalized from an antioxidant with the aid of using receiving a hydrogen atom. The free radicals of this compound produce a purple color and might absorb on the wavelength of 517 nm. Its absorption depth is reduced with the aid of using revitalization and its adjustments to yellow. The antioxidant energy relies upon the discount percent of preliminary darkish red color to the yellow color. The extra is the wide variety of hydroxyl incorporations of antioxidant phenyl loop; the better is the wide variety of hydrogen atoms for response with DPPH and its stabilization. DPPH free radical scavenging impact *C.myrrh* and *C.myrrh*@GNPs in numerous concentrations like 10, 20, 30, 40, 50, 60, 70, 80, 90,

100 $\mu\text{g/ml}$. The observed IC_{50} of *C.myrrh*, DPPH, and *C.myrrh*@GNPs were 100, 93, and 84 respectively (Fig. 16).

3.9. Cell viability against of *C.myrrh* and *C.myrrh*@GNPs

The selected cell lines (HUVEC) were allowed to react with different concentrations of $\text{HAuCl}_4 \cdot 3\text{H}_2\text{O}$, *C.myrrh*, and *C.myrrh*@GNPs in an MTT test used for 48 h regarding the cytotoxic effect on HUVEC cells. The UV–Vis optical density absorbance intensity was identified at 570 nm wavelength, which specifies unexpected absorbance for HUVEC cell line till equal to 1 mg/ml for $\text{HAuCl}_4 \cdot 3\text{H}_2\text{O}$, *C.myrrh*, and *C.myrrh*@GNPs as presented in Fig. 17. On the

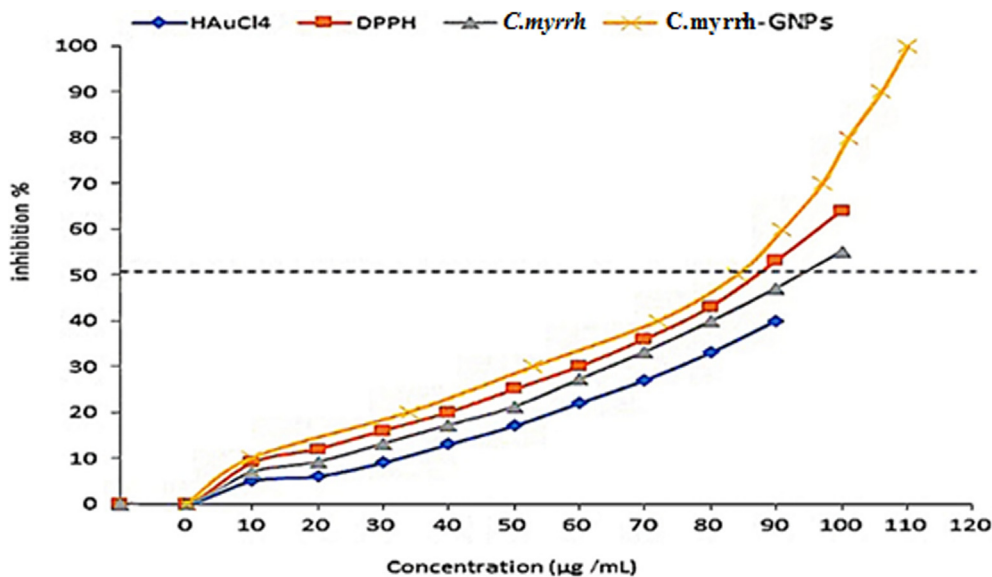


Fig. 16. DPPH free radical scavenging assays of biosynthesized GNPs.

basis of data shown here in figure it clearly indicate that when cell concentration increases, percent viable cell count decreases.

3.10. Cell toxicity study

The *C.myrrh*@GNPs were estimated for their anticancer property towards HCT-116 and MCF-7, by applying an MTT assay. Table 1 disclose that *C.myrrh*@GNPs were efficient towards HCT-116 and MCF-7 cell lines. Different concentrations of *C.myrrh*@GNP like 15 µg, 25 µg, 50 µg, and 100 µg were prepared and treated with the above-mentioned cell lines in the MTT assay. Cell toxicity study was executed to explore the cytotoxic activities of *C.myrrh* and *C.myrrh*@GNPs against cancer cell lines HCT-116 (colon cancer) and MCF-7 (breast cancer). Amazingly, in this study *C.myrrh* did not show considerable cell-toxicity towards selected cancer cell lines (HCT-116 and MCF-7). Cell toxicity against HCT-116 cell line in *C.myrrh*@GNPs was 59.3% for 15 µg/mL, 70.41%, for 25 µg/mL, 85.1 % for 50 µg/mL and highest percent inhibition of 96.5 for 100 µg/mL concentration (Fig. 18(A)). Particularly the cell toxicity against MCF-7 in *C.myrrh*@GNPs was observed highest in 100 µg/mL concentration i.e. 79.92%, 67.43% for 50 µg/mL, 55.20% for 25 µg/mL, 42.37% 15 µg/mL concentrations. Whereas the standard showed 98.18 percent activity as shown in (Fig. 18 (B)). The results of the cell viability and toxicity studies indicated that when concentration increases cell viability and cell toxicity increased. The findings clearly showed the *C.myrrh*@GNPs presents more effective proliferation inhibition percentwise than *C.myrrh* extract shown in Fig. 19 for both the cell lines.

3.11. Anti-inflammatory assay

In this study biosynthesized GNPs were used to inhibit COX-1, and COX-2 by making the different concentrations of *C.myrrh*@GNPs like 25 µg/ml, 50 µg/ml, 100 µg/ml, 200 µg/ml, and

400 µg/ml. The results show that as the *C.myrrh*@GNPs concentration increased the percent inhibition also increased accordingly Fig. 20.

3.12. Antidiabetic

Diabetes mellitus is a metabolic problem caused by abnormalities in insulin release, insulin activity, or both. Therefore, insulin deficiency causes chronic hyperglycemia that adversely affects the digestion of starch, fat, and protein. It is one of the chronic non-communicable diseases (CNCD) that has appeared as a predominant disease in the world. The basis is the investigation of new sources of regular mixtures with potential anti-diabetic effects from tropical greens and nanodevices. An α -amylase is a compound that can break down starch into monomers of glucose. These factors, which are primarily involved in the inhibition of the well-known enzymes α -amylase and α -glucosidase, are of huge significance to diabetes research.

In this study, *C.myrrh*@GNPs were used to inhibit at concentration dependant way to α -amylase and α -glucosidase enzymes. The antidiabetic property of *C.myrrh*@GNPs was found to be increased when a high concentration (400 µg/ml) was used in a dose-dependent manner. The percent inhibition was observed at 50 ± 0.58 and 44 ± 0.49 for α -amylase and α -glucosidase enzymes respectively (Fig. 21).

3.13. Bioassay of antibacterial activities

Medicinal plants contain composite phytochemical components including proteins, saponins, terpenes, alcohols, alkaloids, and phenols, whereas microbes possess key enzymes that can behave as a reducing and stabilizing agent in nanomaterial production. This study reported the antibacterial activity of *C.myrrh*@GNP. The NPs exhibited the highest zone of inhibition towards all four (*Bacil-*

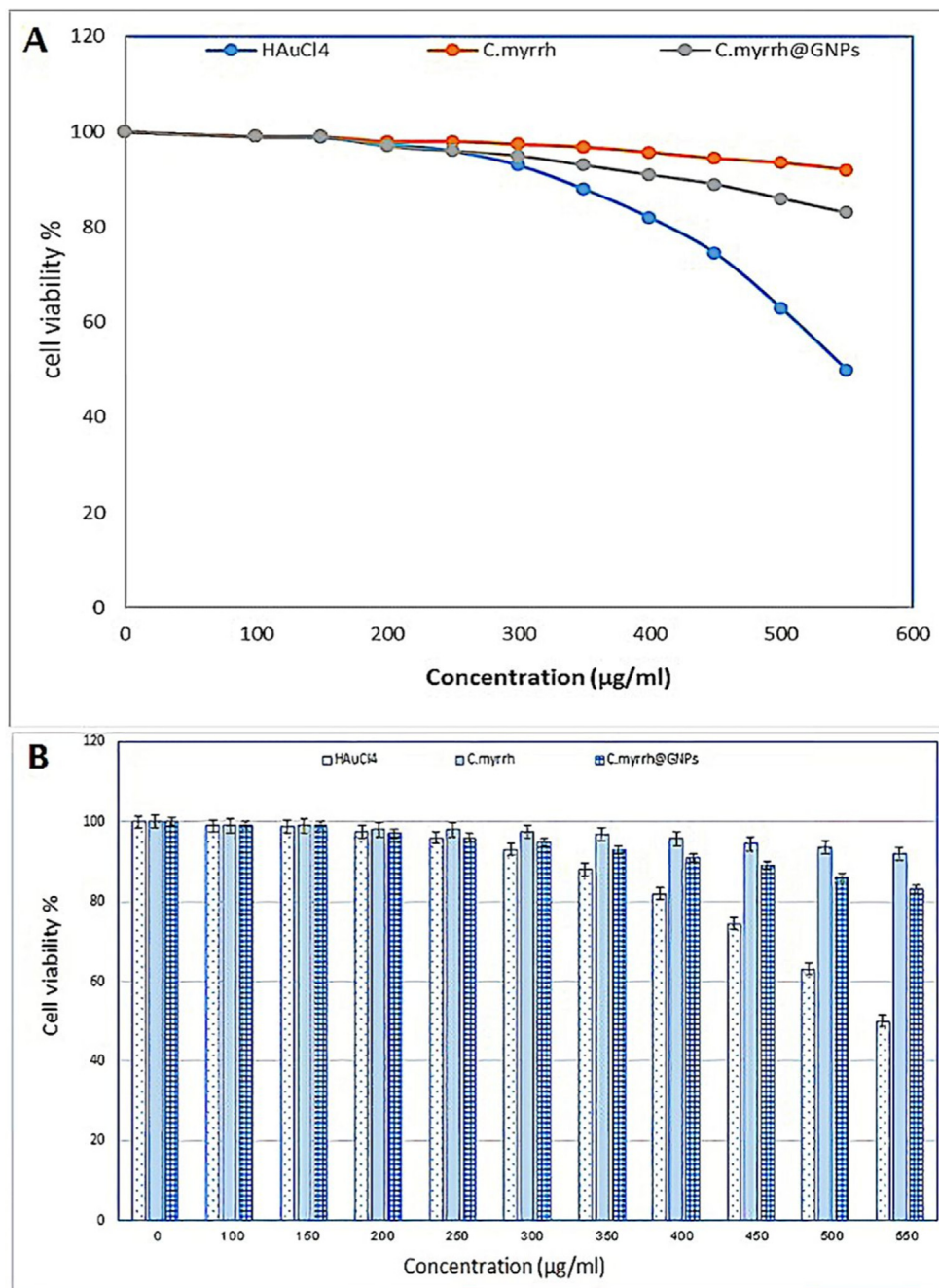


Fig. 17. Percent viability measured on human umbilical vein endothelial cells after treatment with present *C. myrrh*, $HAuCl_3 \cdot 3H_2O$ and *C. myrrh*@GNPs.

Table 1
Inhibitory activity % for HCT-116 and MCF-7 cell line at different concentrations of *C.myrrh*@GNPs.

Sample	Concentration	Standard	C.myrrh	GNPs
HCT-116 Inhibitory activity%	100 µg/mL	99.41	47.50	96.50
	50 µg/mL	95.54	39.40	85.10
	25 µg/mL	92.89	26.53	70.41
	15 µg/mL	90.96	16.43	59.30
MCF-7 Inhibitory activity%	100 µg/mL	98.18	38.32	79.92
	50 µg/mL	93.90	29.22	67.43
	25 µg/mL	91.59	18.69	55.20
	15 µg/mL	90.01	9.89	42.37

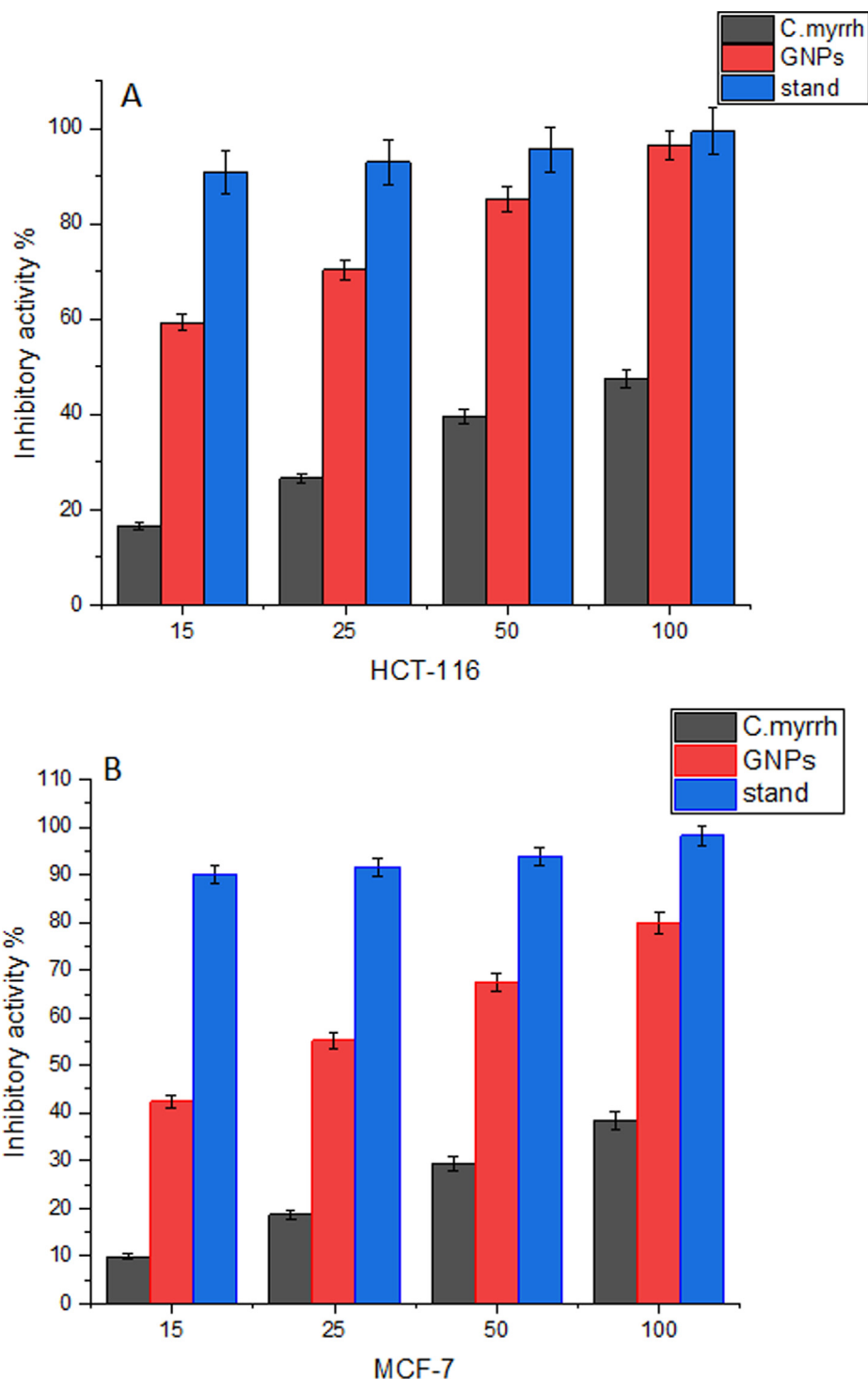


Fig. 18. Inhibitory activity % at different concentrations of *C.myrrh*@GNPs for (A) HCT-116 and (B) MCF-7 cell line.

lus subtilis, *Staphylococcus aureus*, *Pseudomonas aeruginosa*, and *Escherichia coli*) microorganisms utilized. The maximum inhibition varies from 18 ± 0.9 mm to 22 ± 0.5 mm having the uppermost concentration of *C.myrrh*@GNPs next to every pathogen.

The highest inhibition zone was observed to be 22 ± 0.5 mm versus *B. subtilis*, 21 ± 0.1 mm versus *E. coli*, 20 ± 0.7 mm versus *S. aureus*, and 18 ± 0.9 mm versus *P. aeruginosa*. Whereas *C.myrrh* extract showed 17 ± 0.1 mm in *B. subtilis*, 16 ± 0.2 mm in *E. coli*, 15 ± 0.5 mm in *S. aureus*, and 14 ± 0.9 mm in *P. aeruginosa* at a maximum concentration as displayed in Table 2 and Fig. 22.

3.14. Molecular docking

The molecular interaction between drugs and DNA-proteins has been an exciting branch of research in chemical pharmacology and biology (Tian et al., 2008). The important role of peptides as hormones, enzyme inhibitors, neurotransmitters, and immunomodulatory in living systems plays a significant role in the treatment of many diseases (Cruciani et al., 1991; Mai et al., 2001).

The molecular interaction of *C.myrrh* compounds was studied against the three-dimensional complex structure of VEGFR-2

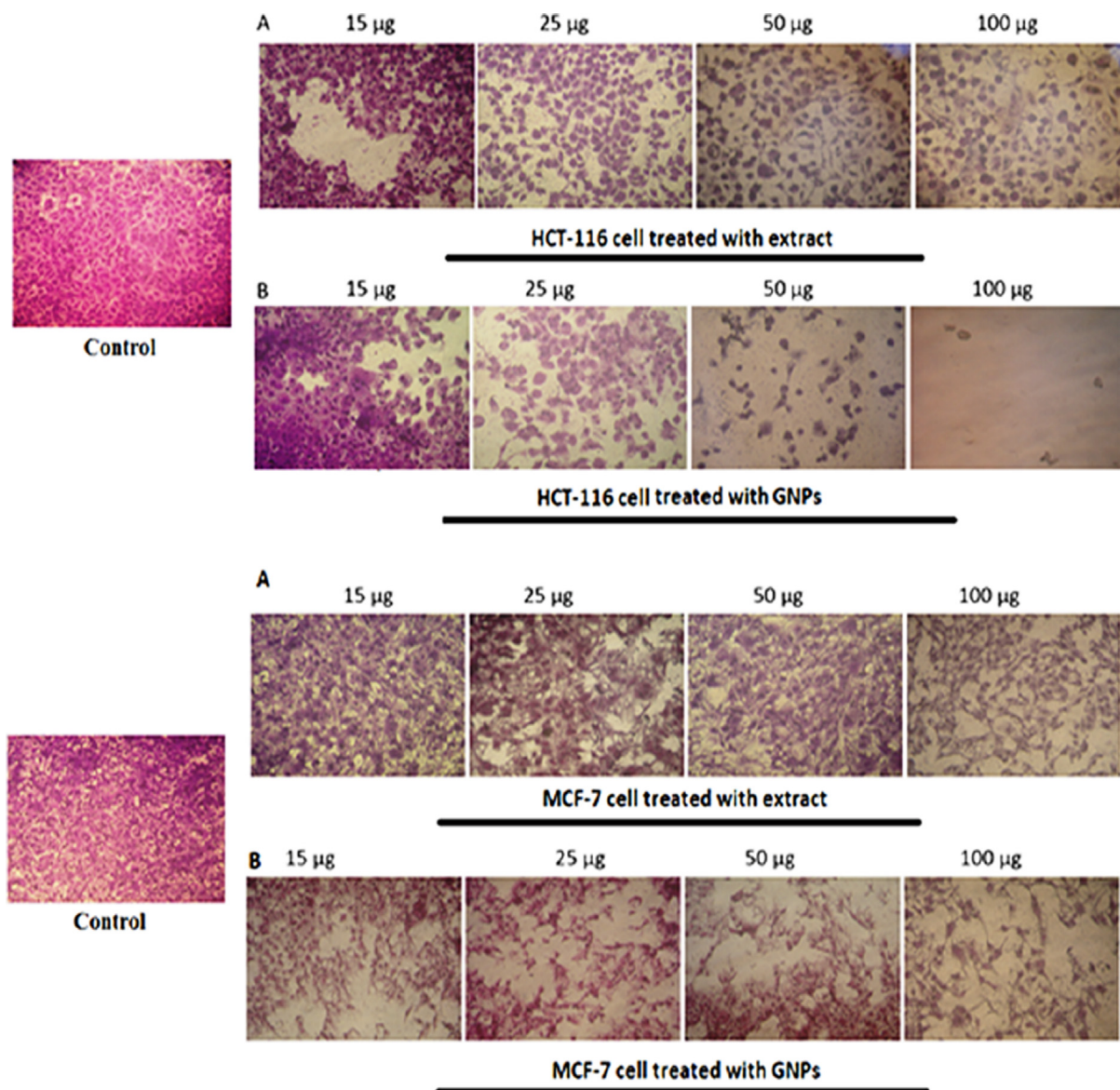


Fig. 19. Inhibition of (HCT-116) and (MCF-7) cell lines by (A) *C.myrrh* and (B) *C.myrrh*@GNPs.

(PDB ID: 1YWN), ovine COX-1 (PDB ID: 3KK6), mouse COX-2 (PDB ID: 3LN1), α -amylase (PDB ID: 4GQR) and α -glucosidase (PDB ID: 5NN5). The obtained results and dock XP G-score and RMSD values (Å) are in Tables 3-7 and shown graphically in Figs. 23-27 and Fig. 1S-36S, supplementary materials.

The interaction of compounds under study can be classified as follow:

- i. Hydrogen bonds to the protein, broken down into backbone and side chain, donor and acceptor.
- ii. Hydrophobic interactions are broken down into π - π stacking (two aromatic groups stacked face-to-face or face-to-edge).
- iii. Water bridge interactions that hydrogen bonding via a water bridge molecule, divided into protein donor and protein acceptor.
- iv. The solvent exposure effect can only decrease binding affinity and it occurs when polar or charged groups of either the compound or protein were exposed to solvent leading to desolvation when being placed in contact with groups to which they cannot hydrogen bond effectively.
- v. No interaction between molecules and the protein.

A cursory a glance at data reported in Tables 3-7 and shown graphically in Figs. 23-27 and Fig. 1S-36S, supplementary materials, one can conclude the following remarks:

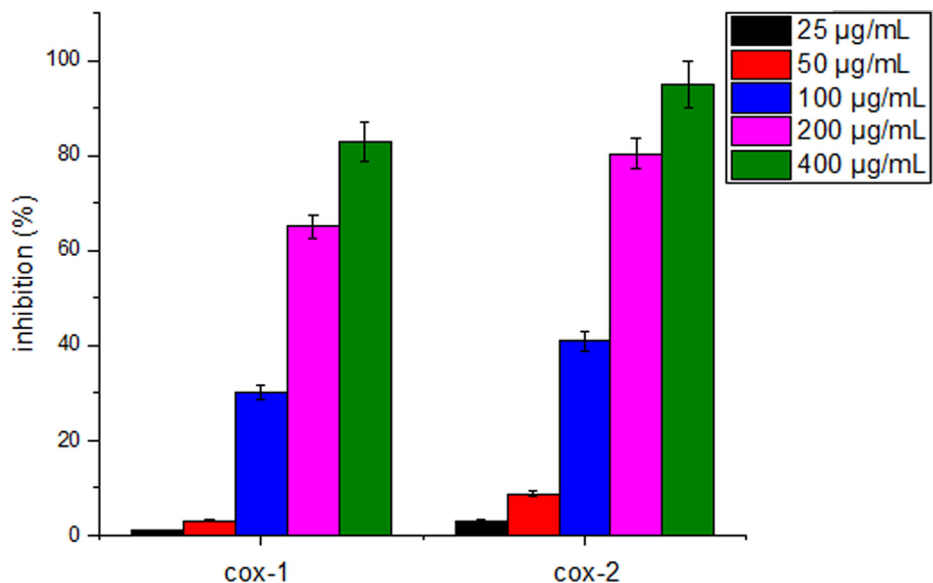


Fig. 20. Anti-inflammatory inhibition of GNP with *C. myrrh* extract.

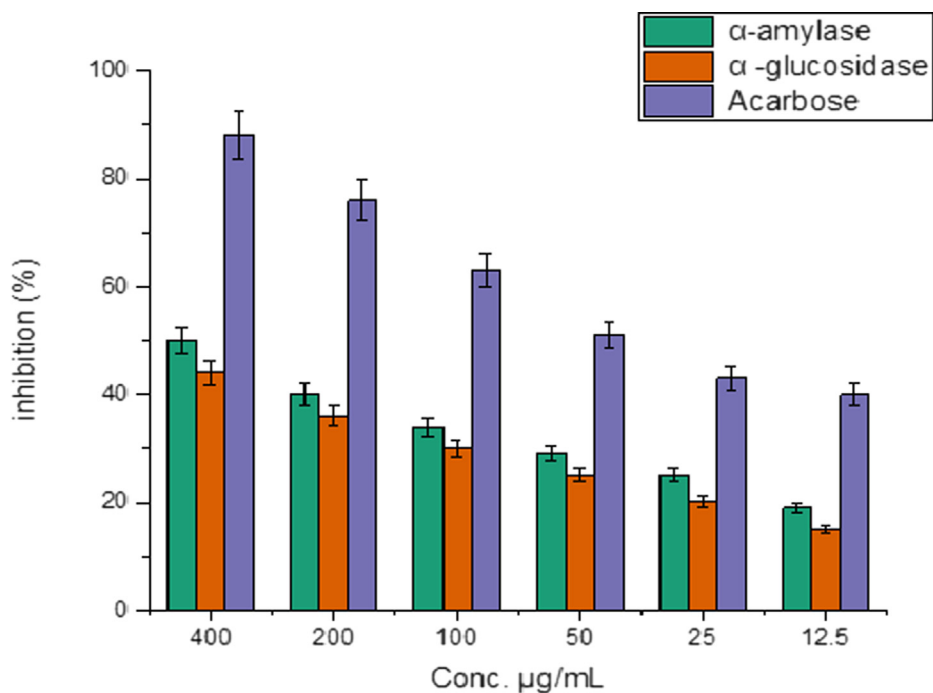


Fig. 21. Anti-diabetic potential of *C. myrrh*@GNPs.

a. All *C. myrrh* compounds have interaction with α -amylase while about 50% of *C. myrrh* compounds have interaction with α -glucosidase which agrees with experimental inhibition of antidiabetics showing that α -amylase is greater than that of α -glucosidase.

b. δ -elemene has the highest dock XP G-score with -3.976 kcal/mol and RMSD = 0.987 Å towards VEGFR-2. Moreover, Furanoedesma-1,3-dien has the highest dock XP G-score with -8.179 kcal/mol and RMSD = 1.128 Å towards COX-1

Table 2
Antibacterial activity (zone of inhibition) from *C.myrrh* and *C.myrrh*@GNPs against positive and negative bacteria.

Microorganisms	Concentration μg/mL	C.myrrh	GNPs
<i>Staphylococcus aureus</i> (ATCC 29213)	15 μg/mL	3 ± 0.3	7 ± 0.2
	25 μg/mL	9 ± 0.1	12 ± 0.9
	50 μg/mL	13 ± 0.1	16 ± 0.3
	100 μg/mL	15 ± 0.5	20 ± 0.7
	Positive control	24 ± 0.6	25 ± 0.6
	Negative control	0.0 ± 0.0	0.0 ± 0.0
<i>Bacillus subtilis</i> (ATCC 6633)	15 μg/mL	5 ± 0.1	8 ± 0.3
	25 μg/mL	11 ± 0.4	15 ± 0.6
	50 μg/mL	14 ± 0.8	19 ± 0.2
	100 μg/mL	17 ± 0.1	22 ± 0.5
	Positive control	25 ± 0.3	24 ± 0.2
	Negative control	0.0 ± 0.0	0.0 ± 0.0
<i>Escherichia coli</i> (ATCC 25922)	15 μg/mL	4 ± 0.3	7 ± 0.6
	25 μg/mL	10 ± 0.1	12 ± 0.5
	50 μg/mL	13 ± 0.8	18 ± 0.7
	100 μg/mL	16 ± 0.2	21 ± 0.1
	Positive control	23 ± 0.6	25 ± 0.6
	Negative control	0.0 ± 0.0	0.0 ± 0.0
<i>Pseudomonas aeruginosa</i> (ATCC 27853)	15 μg/mL	3 ± 0.6	5 ± 0.9
	25 μg/mL	8 ± 0.4	11 ± 0.1
	50 μg/mL	11 ± 0.5	15 ± 0.8
	100 μg/mL	14 ± 0.9	18 ± 0.9
	Positive control	25 ± 0.6	24 ± 0.6
	Negative control	0.0 ± 0.0	0.0 ± 0.0

- c. From the interaction with COX-2 and α -amylase, Lindstrene shows the highest dock XP G-score with -8.200 and -5.581 kcal/mol, respectively resulting from interaction through hydrogen bonds TYR341→(OH) for COX-2 and (OH)→(H₂O) For α -amylase with distances 2.11 and 1.59 Å, respectively
- d. The highest dock XP G-score (-4.293 kcal/mol) with RMSD 1.500 Å for α -glucosidase was appeared with 3,4,4-trimethyl-3-(3-oxobut-1-enyl)bicyclo (4,1,0) heptan-2-on due to hydrogen bond formation ARG600→(C = O) with distance 2.15 Å.
- e. π - π stacking appeared in 2-tert-butyl-1,4-naphthoquinone and curzerene with TYR355 of COX-1. In addition, this interaction appears in Furanodiene with TRP373 of COX-2.
- f. π - π stacking appeared for α -amylase and α -glucosidase in Furanodiene and benzenmethanol-3-methoxy- α -phenyl with TRP59 and TRP481, respectively.
- g. T-Cadinol shows no interaction with VEGFR-2. While benzenmethanol-3-methoxy- α -phenyl has no interaction with both COX-1 and COX-2. Finally, β -elemene, Furanoedesma-1,3-dien, β -Bourbonene, Curzerene, alloaromadendrene, β -Ylangene, α -Selinene, Elemol, Bicyclogermacrene, β -Caryophyllene, and Furanodiene have no interaction with α -glucosidase.

4. Discussion

The aqueous extract of *C.myrrh* indicated the potential for reduction and stabilization of GNPs. When the extract concentration-dependent study was done it is found that the 6 ml extract has the potential to reduce so that the produced NPs possessed a spherical shape.

The absorption maxima were found to be 532 nm this is in the known range of GNPs in scientific research (ElMitwalli et al., 2020; Kumari and Meena, 2020). Here the extract volume also interestingly provides varying results at a small amount of volume, the absorption is very low with broadness, but increasing volume showed increased absorption i.e. 1.3 and the peak also got sharper and narrower so the best volume was at 6 ml and $\lambda_{max} = 532nm$, that range is known for GNPs (Al-Radadi and Al-Youbi, 2018a). Here interesting thing was the salt concentration was only 4 ml where it was given a sharper peak at a wavelength of 532 nm. Comparatively, 3 ml salt concentration exhibited a broad peak and it also shifted which indicated the formation of GNPs it is in collaboration with earlier reports (Burns et al., 2006; Dong et al., 2019). The time optimization study revealed that it completed 80 min to reach a sharper and stabilized absorption maxima at 532nm wavelengths and absorption was observed at more than 2. The curve is narrower and sharper than in the previous report (Al-Radadi and Al-Youbi, 2018b; Huang et al., 2007; Mironava et al., 2010; Sonavane et al., 2008).

The effect of temperature on GNPs was studied and found that at 25 °C higher absorption was received 1.9 and wavelength $\lambda_{max} = 532nm$, which was the narrower and sharper peak than the other temperatures (Al-Radadi, 2022a; Lee et al., 2007; Link and El-Sayed, 1999). A pH dependant study also indicated that direct correlation as pH increased up to a certain level then it becomes decreased. The optimum pH of 4.5 was detected by maximum absorption $\lambda_{max} = 532nm$ (Al-Radadi, 2022b; Okitsu et al., 2009; Singh and Srivastava, 2015; Sun et al., 2009). The size of the *C.myrrh*@GNPs found out that 1.68 nm to 7.86 nm. The Surface Plasmon Resonance (SPR) for *C.myrrh*@GNPs exhibits two contents: first scattering and second absorption. The scattering content is identified as designated for fluorescence improvement while the absorption content is identified as fluorescence quencher (Slocik et al., 2008). The SPR spectrum is dependent on the size, and shape of the NPs, other than additionally being contingent on several outside possessions of the NPs environment like temperature, dielectric constant, medium, and refractive index of the solvent (Umamaheswari et al., 2018). The TEM images showed a circular shape below 10 nm size, this is in collaboration with earlier biosynthesis of GNPs. The NPs are homogenously bounded through a little layer of organic components that are performing as a capping agent (Raliya et al., 2017; Willian et al., 2021). The size was again confirmed by particle size distribution histogram which predicted 4 nm which was also supported by earlier reports on other plant extracts (Al-Radadi, 2021b; Aromal et al., 2012; Barai et al., 2018; Guo et al., 2020). Further elemental gold was confirmed by EDX and the results i.e. presence of 2.8 KeV signal indicated it. These signals were earlier reported by other authors for various plant extract-mediated GNPs (Akintelu et al., 2021; Chen et al., 2021; Naeem et al., 2021). Further XPS confirmed the presence of Au4f_{7/2} and Au4f_{5/2} at 84 eV and 88 eV, separately, indicating the existence of elemental gold and for N1s, C1s and O1s, individually. The C 1s top at 284.5 eV and O1s top at 532.3 eV N1s top at 399.5 eV. These C, N, and O elements were visible may be because of the existence of the amine group in aromatic form, hydrocarbon bunches as well as the carbonyl groups available in polyphenols that made the *C.myrrh*@GNPs stabilized. The existence of such extreme peaks for N, C, and O in XPS analysis later proves the

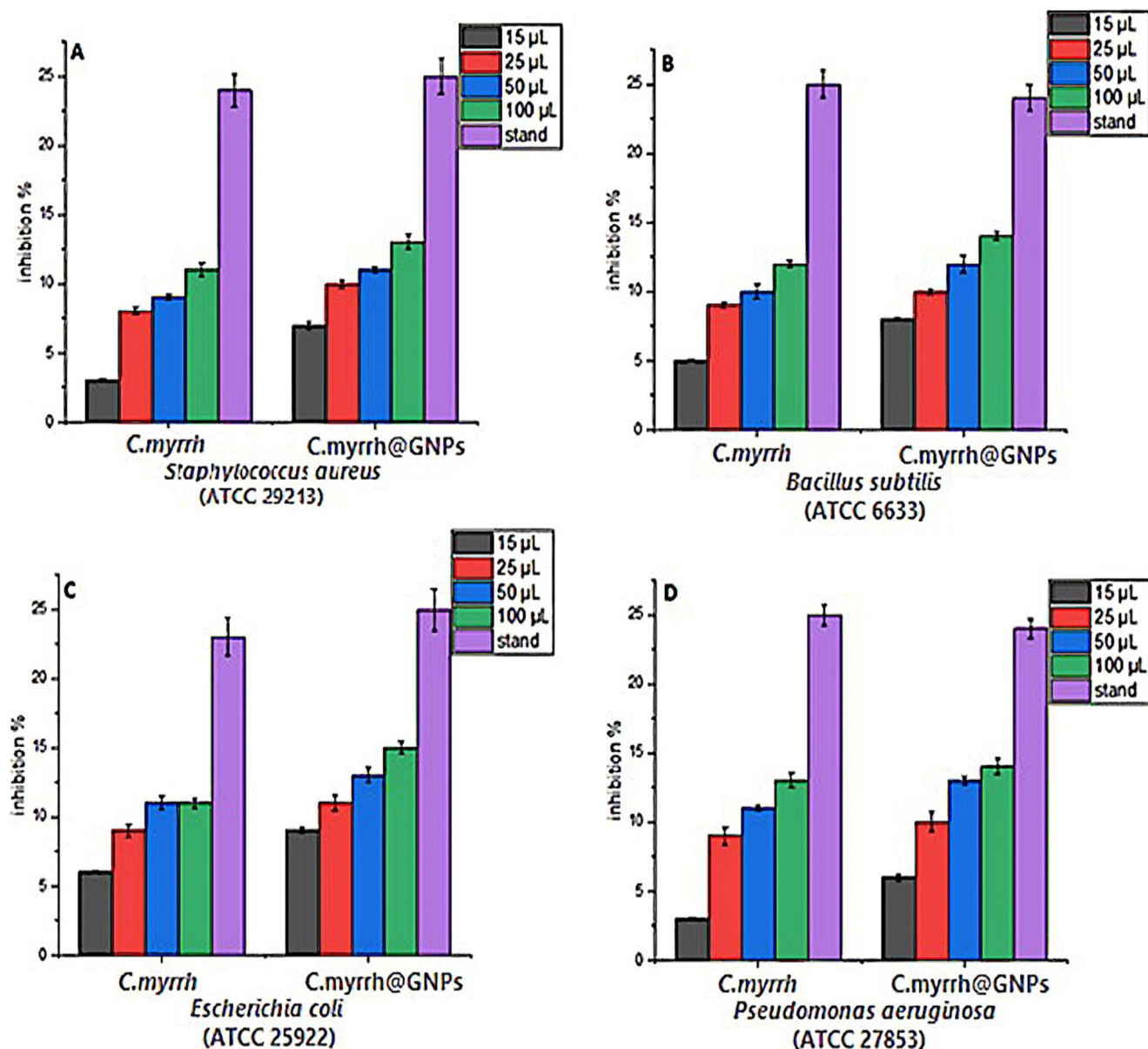


Fig. 22. Inhibitory activity % for Antibacterial at different concentrations of *C.myrrh* and *C.myrrh@GNPs*.

outcomes got from the FTIR examination (Al-Radadi, 2021a; Ahmad et al., 2018; Vijayakumar et al., 2020). In FTIR the C = O (carbonyl gatherings) and hydroxide may be liable for the arrangement of the NPs and may assume a significant part in the adjustment of the shape of GNPs. The flavonoids that existed in the *C. myrrh* seed extract were a strong reducing potential which might be responsible for the reduction of gold salt. Hence it is observed that *C.myrrh* extract can fill double roles of reducing and stabilizing agent for *C.myrrh@GNPs* earlier reports of other plant extract showed if these molecules are present then its extract works as a dual function (Clarance et al., 2020; Shejawal et al., 2021; Yas et al., 2021). The *C.myrrh@GNPs* was examined for crystallography using X-ray diffraction and found four major peaks of 2θ at 38.1, 44.5, 65, 78, and fifth at 82 which were allocated to (111), (200), (220), (311) and (222) crystalline planes respectively of gold. The peak ensuing to (111) was sufficiently tough as compared to other present planes suggesting that the *C.myrrh* extract produced crystalline GNP has crystalline nature and (111) was observed principal orientation (Al-Radadi, 2022b; Parida et al.,

2011). The stability of the NPs was examined through DLS which was found to be (-10.8) mV. There was a discrepancy in TEM size and DLS size analysis of *C.myrrh@GNP* it is well known that DLS determines radii of gold and might the organic compounds surrounded by the GNPs synthesized by *C.myrrh* (Al-Radadi, 2021b; Khan et al., 2020; Perveen et al., 2021; Vijayakumar et al., 2020). The free radical scavenging activity using DPPH showed good improvement as compared to *C.myrrh* extract and its GNPs. Different concentrations such as from 10 to 100 µg/ml. The determined IC_{50} values for *C.myrrh*, DPPH, and *C.myrrh@GNPs* were 100, 93, and 84 correspondingly (Al-Radadi, 2021a; Khan et al., 2020). These findings are consistent with the earlier reports for different plants (Al-Radadi, 2022c; Kiran et al., 2021; Satpathy et al., 2020; Zhang et al., 2020) which presented that the plant extract while reacting with metal salts it loses its cytotoxicity (Al-Radadi, 2022b; Al-Radadi, 2021a; Mai et al., 2021; Parida et al., 2014). Anticancer activity against breast and colon cell lines showed a dose-dependent response. Amongst the different concentrations utilized 100 µg/ml concentration was inhibitory the concentration of

Table 3
Molecular interactions of *C.myrrh* compounds predicted for inhibitor binding to VEGFR-2.

Compound	Docking score	RMSD (Å)	Interaction		
			Bond	Type	distance (Å)
δ-elemene	-3.976	0.987	-	-	-
Furanoedesma-1,3-dien	-3.912	0.967	-	-	-
β-Bourbonene	-3.806	1.199	Solvent exposure	-	-
menthofuran	-3.568	1.188	(H ₂ O)→(C-O)hetero-ring	H-Bond	2.21
3,4,4-trimethyl-3-(3-oxobut-1-enyl)bicyclo(4,1,0)heptan-2on	-3.537	1.480	ASP1044→(C = O)	H-Bond	2.22
γ-Elemene	-3.507	0.970	-	-	-
2-tert-butyl-1,4-naphthoquinone	-3.449	1.083	-	-	-
α-Humulene	-3.433	0.958	-	-	-
Curzerene	-3.371	0.921	-	-	-
allo-Aromadendrene	-3.325	1.141	Solvent exposure	-	-
β-Ylangene	-3.222	0.764	Solvent exposure	-	-
benzenmethanol-3-methoxy-α-phenyl	-3.205	0.887	(OH)→(H ₂ O)	H-Bond	1.69
β-Selinene	-3.165	1.259	Solvent exposure	-	-
β-elemene	-3.160	0.790	Solvent exposure	-	-
Elemol	-3.160	0.757	(OH) → ASP1044	H-Bond	1.93
γ-Murolene	-2.951	1.502	-	-	-
Bicyclogermacrene	-2.805	1.228	-	-	-
β-Caryophyllene	-2.709	1.869	-	-	-
α-selinene	-2.642	1.375	Solvent exposure	-	-
α-Copaene	-2.488	1.353	Solvent exposure	-	-
Lindestrene	-2.425	1.788	Solvent exposure	-	-
2-methoxyFuranodiene	-2.287	0.764	Solvent exposure	-	-
Furanodiene	-1.655	1.390	Solvent exposure	-	-
T-Cadinol	No interaction	-	-	-	-

Table 4
Molecular interactions of *C.myrrh* compounds predicted for inhibitor binding to COX-1.

Compound	Docking score	RMSD (Å)	Interaction		
			Bond	Type	distance (Å)
Furanoedesma-1,3-dien	-8.179	1.218	-	-	-
Furanodiene	-7.834	1.664	-	-	-
δ-elemene	-7.436	1.029	-	-	-
β-Caryophyllene	-7.411	1.685	-	-	-
2-tert-butyl-1,4-naphthoquinone	-7.206	0.927	Aromatic ring-TYR355	π-π stacking	5.33
Lindestrene	-6.866	0.905	-	-	-
β-Ylangene	-6.854	1.372	-	-	-
γ-Murolene	-6.750	0.904	-	-	-
β-elemene	-6.666	1.074	-	-	-
α-selinene	-6.523	1.039	-	-	-
β-Selinene	-6.516	0.894	-	-	-
α-Copaene	-6.506	0.462	-	-	-
α-Humulene	-6.384	0.694	-	-	-
β-Bourbonene	-6.345	0.767	-	-	-
Bicyclogermacrene	-6.338	1.292	-	-	-
Menthofuran	-6.185	0.981	-	-	-
γ-Elemene	-6.044	0.655	-	-	-
allo-Aromadendrene	-5.986	0.870	-	-	-
Curzerene	-5.720	1.693	ARG120→(C-O)ring	H-Bond	1.83
3,4,4-trimethyl-3-(3-oxobut-1-enyl)bicyclo(4,1,0)heptan-2on	-5.532	0.861	Furan ring-TYR355	π-π stacking	4.61
T-cadinol	-5.411	0.871	-	-	-
Elemol	-5.359	1.693	-	-	-
2-methoxyFuranodiene	-3.802	0.931	Solvent exposure	-	-
benzenmethanol-3-methoxy- α-phenyl	No interaction	-	-	-	-

C.myrrh@GNPs for which it is found excellent inhibition as compared to *C.myrrh* extract. These outcomes recommended that the anticancer activity designate concentration and dose-dependent (Al-Radadi, 2022c; Perveen et al., 2021; Al-Radadi, 2021a; Shejawal et al., 2021; Siegel et al., 2013; Anand et al., 2015; Wang et al., 2019). The inflammatory study was also carried out which showed that the GNPs were used to inhibit COX-1, and COX-2, it is found that the response was having direct contact with the concentration of *C.myrrh*@GNPs here it is observed that 400 µg/ml concentration showed excellent inhibition of COX-1 and COX-2. These results exhibited that the phenolics and flavonoids in *C.myrrh* extract impart excellent anti-inflammatory stress via

numerous mechanisms (Al-Radadi, 2022b; Hwang et al., 2015; Singh et al., 2018). The *C.myrrh*@GNPs used to treat α-amylase and α-glucosidase enzymes to detect the anti-diabetic property of *C.myrrh*@GNPs was found to be increased when concentration was increased. The 400 µg/ml was used in a dose-dependent manner. The percent inhibition was observed at 50 ± 0.58 and 44 ± 0.49 for α-amylase and α-glucosidase enzymes respectively (Al-Radadi, 2022b; Kiran et al., 2021; Senthilkumar et al., 2019; Vijayakumar et al., 2020). The findings of the antibacterial study exhibited that the *C.myrrh*@GNPs at 100 µg/ml concentrations may retard the bacterial growth of pathogens liable for food toxicity (Al-Radadi, 2021b; Siegel et al., 2013). The medicinal value also reported the

Table 5
Molecular interactions of *C.myrrh* compounds predicted for inhibitor binding to COX-2.

Compound	Docking score	RMSD (Å)	Interaction		
			Bond	Type	distance (Å)
Lindrestrene	-8.200	1.660	TYR341 →(OH)	H-Bond	2.11
α-Humulene	-8.028	1.107	-	-	-
Furanouedesma-1,3-dien	-7.827	1.163	-	-	-
γ-Elemene	-7.438	0.878	-	-	-
δ-elemene	-7.330	1.386	-	-	-
β-Caryophyllene	-7.245	1.670	-	-	-
T-cadinol	-7.134	1.062	-	-	-
Curzerene	-7.121	0.975	-	-	-
Furanodiene	-7.098	1.151	TRP373—furan ring	π-π stacking	5.35
β-Selinene	-6.950	0.889	-	-	-
Elemol	-6.644	0.779	TYR341 →(OH)	H-Bond	2.21
3,4,4-trimethyl-3-(3-oxobut-1-enyl)bicyclo(4,1,0)heptan-2on	-6.638	1.061	TYR341 →(C = O)	H-Bond	2.70
2-tert-butyl-1,4-naphthoquinone	-6.615	1.237	-	-	-
β-elemene	-6.552	1.120	-	-	-
allo-Aromadendrene	-6.504	1.070	-	-	-
menthofuran	-6.486	1.034	-	-	-
β-Bourbonene	-6.382	1.224	-	-	-
α-selinene	-6.354	1.482	-	-	-
β-Ylangene	-6.267	0.968	-	-	-
Bicyclgermacrene	-5.955	1.216	-	-	-
γ-Murolene	-5.944	0.858	-	-	-
α-Copaene	-5.053	0.601	-	-	-
2-methoxyFuranodiene	-4.206	0.849	Solvent exposure	-	-
benzenmethanol-3-methoxy-α-phenyl	No interaction	-	-	-	-

Table 6
Molecular interactions of *C.myrrh* compounds predicted for inhibitor binding to α-amylase.

Compound	Docking score	RMSD (Å)	Interaction		
			Bond	Type	distance (Å)
Lindrestrene	-5.581	1.008	(OH)→(H ₂ O)	H-Bond	1.59
Furanodiene	-4.603	1.112	Furan ring—TRP59	π-π stacking	3.78, 3.94
Furanouedesma-1,3-dien	-4.564	0.691	(H ₂ O)→(C-O) _{Furan ring}	H-Bond	2.41
2-tert-butyl-1,4-naphthoquinone	-4.559	0.832	GLN63→(C = O)	H-Bond	1.95
β-Caryophyllene	-4.355	1.192	-	-	-
Curzerene	-4.195	1.500	Solvent exposure	-	-
α-selinene	-4.080	0.831	-	-	-
Elemol	-4.021	1.065	(OH)→(H ₂ O)	H-Bond	1.86
γ-Elemene	-4.013	1.242	Solvent exposure	-	-
β-Ylangene	-3.982	0.990	-	-	-
β-Selinene	-3.976	1.241	Solvent exposure	-	-
α-Humulene	-3.955	0.963	Solvent exposure	-	-
β-Bourbonene	-3.898	0.830	Solvent exposure	-	-
3,4,4-trimethyl-3-(3-oxobut-1-enyl)bicyclo(4,1,0)heptan-2on	-3.894	0.817	(H ₂ O)→(C = O)	H-Bond	2.43
menthofuran	-3.857	1.146	GLN63→(C-O) _{Furan ring}	H-Bond	2.25
β-elemene	-3.856	0.722	Solvent exposure	-	-
α-Copaene	-3.822	0.717	Solvent exposure	-	-
Bicyclgermacrene	-3.754	0.872	Solvent exposure	-	-
T-cadinol	-3.737	1.802	Solvent exposure	-	-
δ-elemene	-3.671	1.341	-	-	-
allo-Aromadendrene	-3.624	0.568	Solvent exposure	-	-
γ-Murolene	-3.590	1.240	Solvent exposure	-	-
benzenmethanol-3-methoxy-α-phenyl	-3.508	0.951	(OH)→(H ₂ O) → THR163	H-Bond via water molecule	2.13, 2.30
2-methoxyFuranodiene	-3.120	0.840	(C-O)→(H ₂ O) → THR163	H-Bond via water molecule	2.09, 2.30

effect of *C.myrrh* extract against the diabetics and antibacterial but here GNPs capped with the *C.myrrh* extract have shown the excellent report on diabetic and antibacterial activity (Khalil et al, 2020; Al-Radadi, 2022b). The reason for this antibacterial activity is that the *C.myrrh* extract contains many phytochemicals that were capped around the GNPs (Al-Radadi, 2022c).

5. Future perspective

Some antibacterial, anti-inflammatory and anti-diabetic medications are being repurposed in clinical trials globally and several potential findings been lately been stated. In this case, NPs attract the center and are thought to be a viable substitute. Additionally,

Table 7
Molecular interactions of *C.myrrh* compounds predicted for inhibitor binding to α -glucosidase.

Compound	Docking score	RMSD (Å)	Interaction		
			Bond	Type	distance (Å)
3,4,4-trimethyl-3-(3-oxobut-1-enyl)bicyclo(4,1,0)heptan-2on	-4.293	1.500	ARG600→(C = O)	H-Bond	2.15
T-cadinol	-4.245	1.715	(OH) → ASP616	H-Bond	1.49
α -Humulene	-3.952	1.697	-	-	-
α -Copaene	-3.243	1.826	Solvent exposure	-	-
β -Selinene	-3.195	1.897	Solvent exposure	-	-
benzenmethanol-3-methoxy- α -phenyl	-2.684	1.083	(OH) → ASP282	H-Bond	1.95
			Aromatic ring—TRP481	π - π stacking	5.28
δ -elemene	-2.515	1.187	-	-	-
γ -Muroloene	-1.857	1.148	Solvent exposure	-	-
Lindestrene	-1.757	0.968	TRP618→(H ₂ O)→(C = O)	H-Bond via water molecule	1.98, 2.11
2-methoxyFuranodiene	-1.477	1.126	TRP618→(H ₂ O)→(C-O)	H-Bond via water molecule	1.98, 2.11
2- <i>tert</i> -butyl-1,4-naphthoquinone	-1.373	1.126	ALA284→(C = O)	H-Bond	2.33
menthofuran	-0.090	0.964	TRP618→(H ₂ O)→(C-O)	H-Bond via water molecule	1.98, 2.18
γ -Elemene	1.254	1.000	Solvent exposure	-	-
β -elemene	No interaction	-	-	-	-
Furanoeudesma-1,3-dien	No interaction	-	-	-	-
β -Bourbonene	No interaction	-	-	-	-
Curzerene	No interaction	-	-	-	-
allo-Aromadendrene	No interaction	-	-	-	-
β -Ylangene	No interaction	-	-	-	-
α -Selinene	No interaction	-	-	-	-
Elemol	No interaction	-	-	-	-
Bicyclogermacrene	No interaction	-	-	-	-
β -Caryophyllene	No interaction	-	-	-	-
Furanodiene	No interaction	-	-	-	-

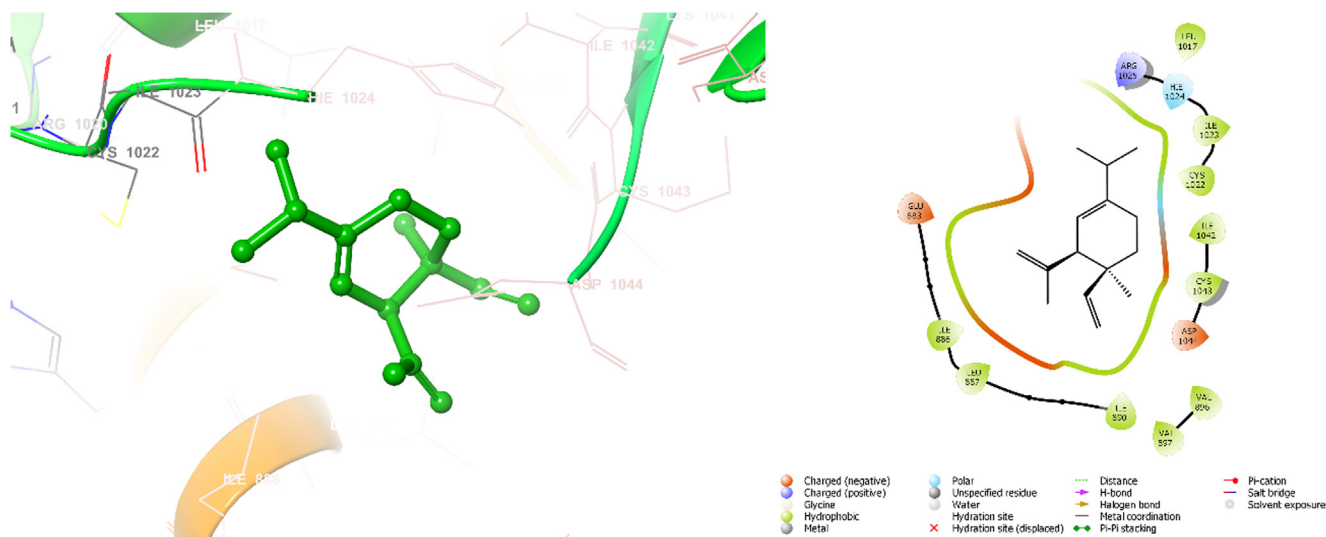


Fig. 23. 3D and 2D molecular interaction of δ -elemene for inhibitor to VEGFR-2.

C.myrrh@GNP found potential findings that these NPs can be applied against pathogenic bacteria, as an anti-inflammatory and anti-diabetic, as well as anticancer agent. The *C.myrrh*@GNP is currently exhibiting the potential revolutionary agent which will create a constructive and encouraging impact on biomedical fields in the future.

6. Conclusions

The *C.myrrh* is of high medicinal importance, This method of synthesis of GNPs will obviously increase the total medicinal value of the GNPs capped by *C.myrrh* biomolecules. The overall finding of the work enlightens the medicinal importance of *C.myrrh*@GNPs.

The method is the most effective method, regarding price, and energy and it also exhibits simplicity. GNPs characterized by spectroscopic and microscopic techniques revealed that there is a direct correlation between volume and SPR peak of the synthesized GNP. The size structure and morphology of the nanomaterials are spherical, crystalline, and with an average size of 4 nm, made up of metallic gold. The functional molecules surrounding the surface of the NPs are coming from the *C.myrrh* extract and contributing to the cell toxicity, anti-biotic (antibacterial), anti-inflammatory antidiabetic and antioxidant properties. *C.myrrh*@GNPs demonstrated a remarkable cell line proliferation inhibition activity against MCF-7 and HCT-116 cell lines. The molecular docking of Polyphenol exhibits the high affinity of Polyphenol against HCT-116, inflammatory and diabetic.

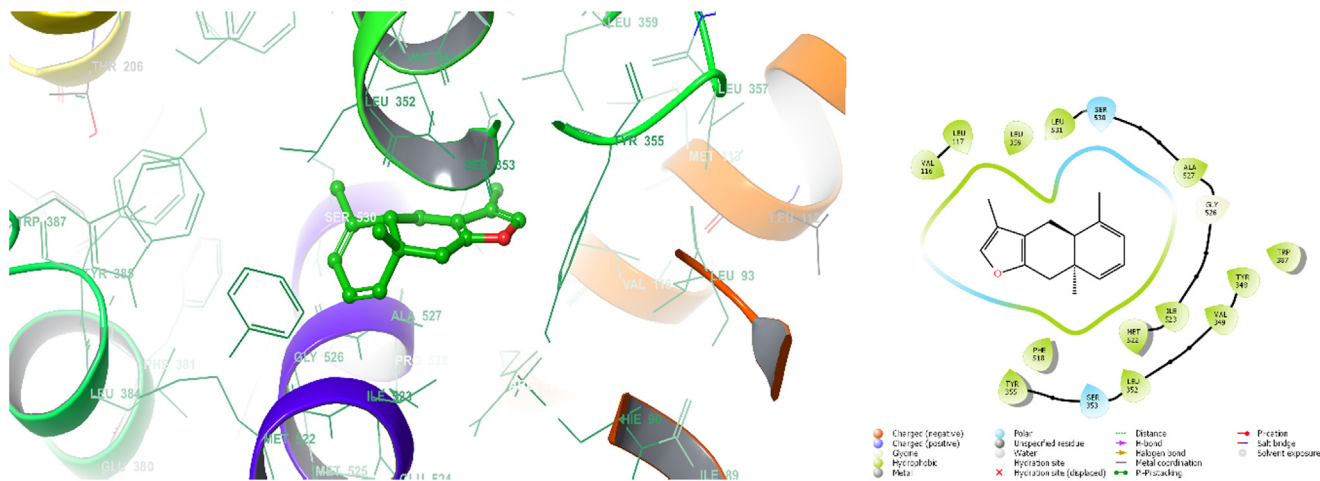


Fig. 24. 3D and 2D molecular interaction of Furanoedesma-1,3-dien for inhibitor to COX-1.

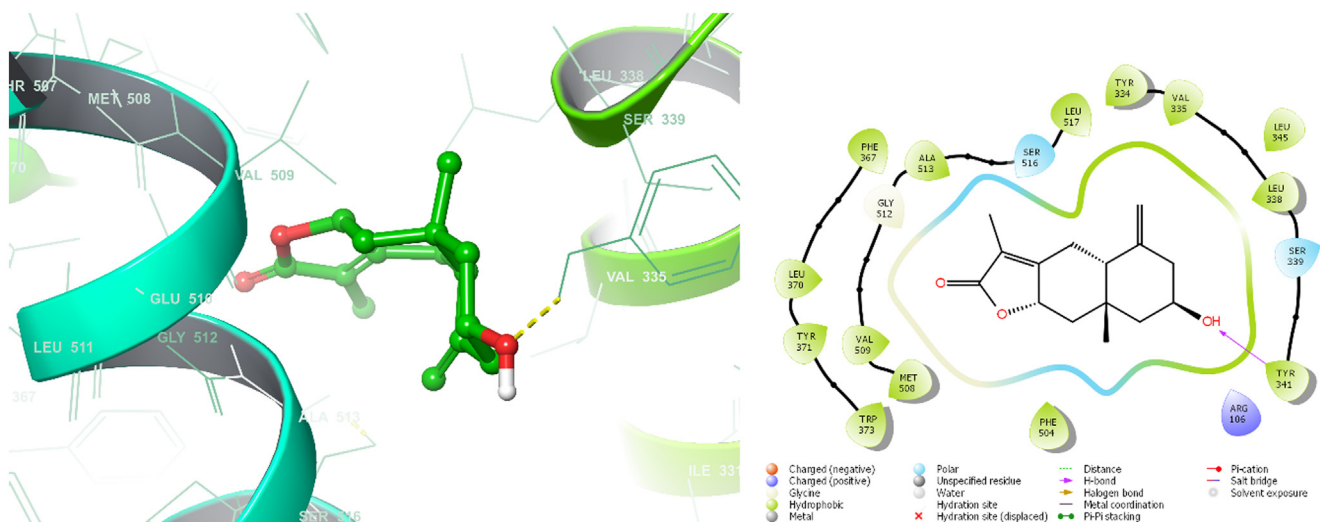


Fig. 25. 3D and 2D molecular interaction of Lindrestrene for inhibitor to COX-2.

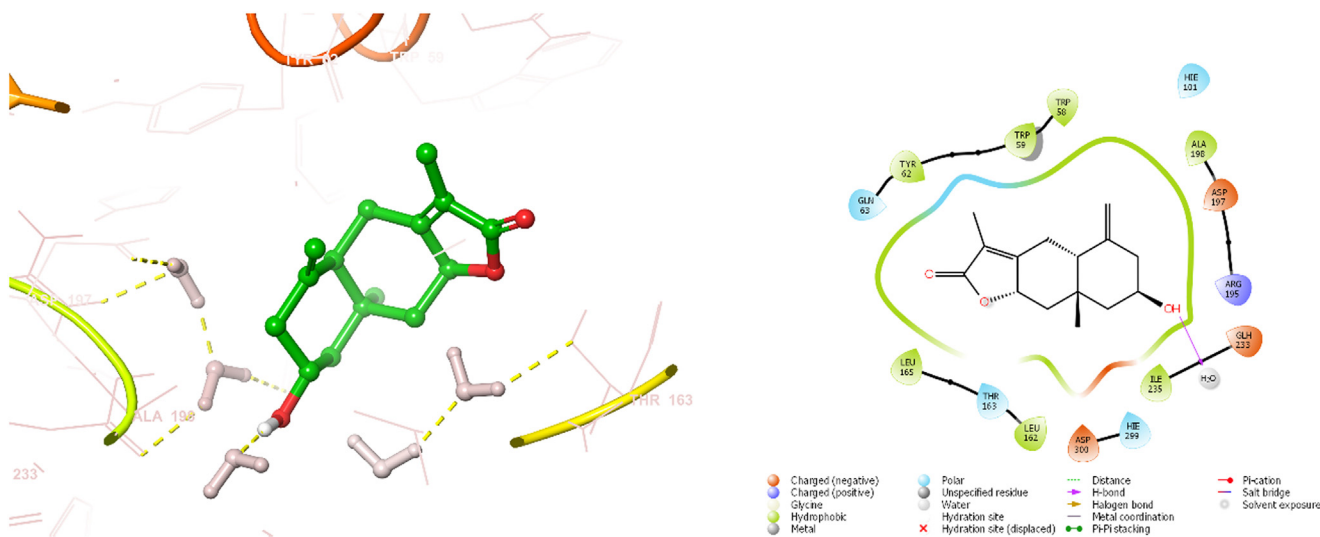


Fig. 26. 3D and 2D molecular interaction of Lindrestrene for inhibitor to α -amylase.

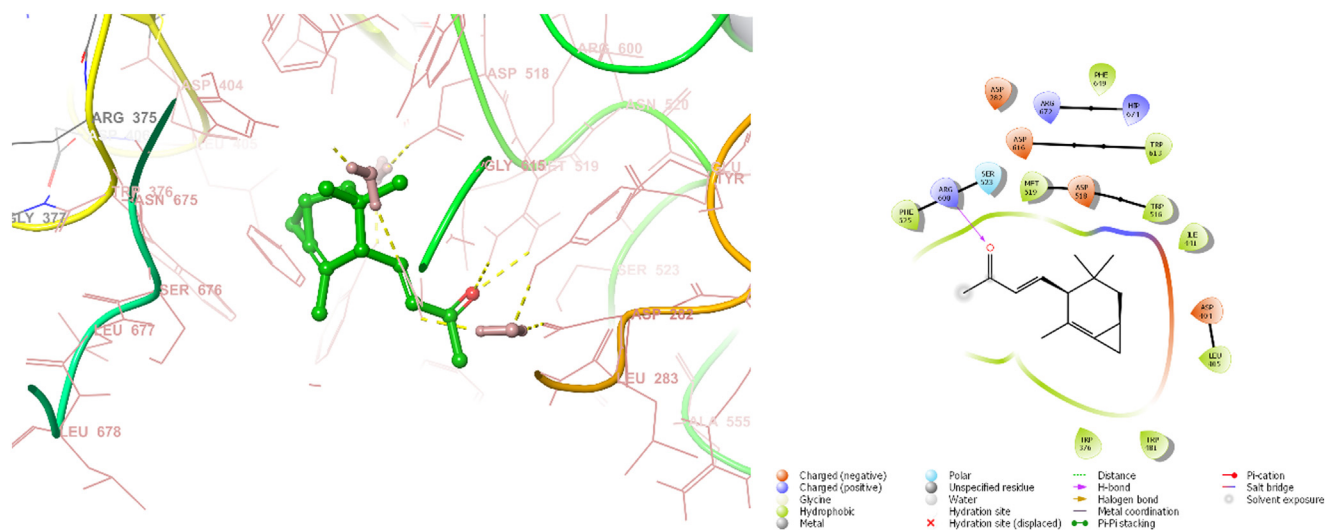


Fig. 27. 3D and 2D molecular interaction of 3,4,4-trimethyl-3-(3-oxobut-1-enyl)bicyclo(4,1,0)heptan-2-one for inhibitor to α -glucosidase.

Funding

No fund was taken from any source.

Declaration of Competing Interest

The authors declare that they have no known competing financial interests or personal relationships that could have appeared to influence the work reported in this paper.

Appendix A. Supplementary data

Supplementary data to this article can be found online at <https://doi.org/10.1016/j.jsps.2022.06.028>.

References

- Abdelbasir, S.M., Shalan, A.E., 2019. An overview of nanomaterials for industrial wastewater treatment. *Korean J. Chem. Eng.* <https://doi.org/10.1007/s11814-019-0306-y>.
- Abdullah, A.-R., Hussain, T., Faisal, S., Ali Raza Shah, S., 2021. Novel biosynthesis, characterization and bio-catalytic potential of green algae (*Spirogyra hyalina*) mediated silver nanomaterials. *Saudi J. Biol. Sci.* <https://doi.org/10.1016/j.sjbs.2021.09.013>.
- Ahmad, T., Bustam, M.A., Irfan, M., Moniruzzaman, M., Anwaar Asghar, H.M., Bhattacharjee, S., 2018. Green synthesis of stabilized spherical shaped gold nanoparticles using novel aqueous *Elaeis guineensis* (oil palm) leaves extract. *J. Mol. Struct.* 1159, 167–173. <https://doi.org/10.1016/j.molstruc.2017.11.095>.
- Akintelu, S.A., Yao, B., Folorunso, A.S., 2021. Green Synthesis, Characterization, and Antibacterial Investigation of Synthesized Gold Nanoparticles (AuNPs) from *Garcinia kola* Pulp Extract. *Plasmonics* 16, 157–165. <https://doi.org/10.1007/s11468-020-01274-9>.
- Al-Awadi, F.M., Gumaa, K.A., 1987. Studies on the activity of individual plants of an antidiabetic plant mixture.
- Albrecht, M.A., Evans, C.W., Raston, C.L., 2006. Green chemistry and the health implications of nanoparticles. *Green Chem.* 8, 417–432. <https://doi.org/10.1039/b517131h>.
- Al-Harbi, M.M., Qureshi, S., Raza, M., Ahmed, M.M., Afzal, M., Shah, A.H., 1997. Gastric antiulcer and cytoprotective effect of *Commiphora molmol* in rats. *J. Ethnopharmacol.* 55. [https://doi.org/10.1016/S0378-8741\(96\)01488-2](https://doi.org/10.1016/S0378-8741(96)01488-2).
- Al-Radadi, N.S., 2022a. Microwave Assisted Green Synthesis of Fe@Au Core-Shell NPs Magnetic to Enhance Olive oil Efficiency on Eradication of *Helicobacter pylori* (Life preserver). *Arabian J. Chem.* <https://doi.org/10.1016/j.arabjc.2022.103685>.
- Al-Radadi, N.S., 2022b. Biogenic Proficient Synthesis of (Au-NPs) via Aqueous Extract of Red Dragon Pulp and Seed Oil: Characterization, Antioxidant, Cytotoxic properties, Anti-diabetic Antiinflammatory, Anti-Alzheimer and their Anti-proliferative Potential against cancer Cell Lines. *Saudi J. Biol. Sci.* <https://doi.org/10.1016/j.sjbs.2022.01.001>.
- Al-Radadi, N.S., 2022c. Laboratory Scale Medicinal Plants Mediated Green Synthesis of Biocompatible Nanomaterials and their Versatile Biomedical Applications. *Saudi J. Biol. Sci.* <https://doi.org/10.1016/j.sjbs.2022.02.042>.
- Al-Radadi, N.S., 2021a. Green Biosynthesis of Flaxseed Gold Nanoparticles (Au-NPs) as Potent Anti-cancer Agent Against Breast Cancer Cells. *Journal of Saudi Chemical Society* 25. <https://doi.org/10.1016/j.jscs.2021.101243>.
- Al-Radadi, N.S., 2021b. Facile one-step green synthesis of gold nanoparticles (AuNp) using licorice root extract: Antimicrobial and anticancer study against HepG2 cell line. *Arabian J. Chem.* 14. <https://doi.org/10.1016/j.arabjc.2020.102956>.
- Al-Radadi, N.S., 2019. Green synthesis of platinum nanoparticles using Saudi's Dates extract and their usage on the cancer cell treatment. *Arabian J. Chem.* 12, 330–349. <https://doi.org/10.1016/j.arabjc.2018.05.008>.
- Al-Radadi, N.S., 2018. Artichoke (*Cynara scolymus* L.), mediated rapid analysis of silver nanoparticles and their utilisation on the cancer cell treatments. *J. Comput. Theor. Nanosci.* 15, 1818–1829. <https://doi.org/10.1166/jctn.2018.7317>.
- Al-Radadi, N.S., Abdullah, et al., 2022. Zingiber officinale driven bioproduction of ZnO nanoparticles and their anti-inflammatory, anti-diabetic, anti-Alzheimer, anti-oxidant, and anti-microbial applications. *Inorganic. Chem. Commun.* 140. <https://doi.org/10.1016/j.inoche.2022.109274>.
- Al-Radadi, N.S., Adam, S.I.Y., 2020. Green biosynthesis of Pt-nanoparticles from Anbara fruits: Toxic and protective effects on CCl4 induced hepatotoxicity in Wister rats. *Arabian J. Chem.* 13, 4386–4403. <https://doi.org/10.1016/j.arabjc.2019.08.008>.
- Al-Radadi, N.S., Al-Youbi, A.N., 2018a. Environmentally-safe synthesis of gold and silver nano-particles with AL-madinah Barni fruit and their applications in the cancer cell treatments. *J. Comput. Theor. Nanosci.* 15, 1853–1860. <https://doi.org/10.1166/jctn.2018.7322>.
- Al-Radadi, N.S., Al-Youbi, A.N., 2018b. One-step synthesis of au nano-assemblies and study of their anticancer activities. *J. Comput. Theor. Nanosci.* 15, 1861–1870. <https://doi.org/10.1166/jctn.2018.7323>.
- Al-Radadi, N.S., Abu-Dief, 2022. Silver nanoparticles (AgNPs) as a metal nanotherapy: possible mechanisms of antiviral action against COVID-19. *INORGANIC AND NANO-METAL CHEMISTRY..* <https://doi.org/10.1080/24701556.2022.2068585>.
- Al Jahdaly, B.A., Al-Radadi, N.S., et al., 2021. Selenium nanoparticles synthesized using an eco-friendly method: dye decolorization from aqueous solutions, cell viability, antioxidant, and antibacterial effectiveness. *J. mater. res. tech.* 11, 85–90.
- Arulmozhi, V., Pandian, K., Mirunalini, S., 2013. Ellagic acid encapsulated chitosan nanoparticles for drug delivery system in human oral cancer cell line (KB). *Colloids Surf., B* 110, 313–320.
- Alwhibi, M.S., Soliman, D.A., al khalidy, H., Alonzaian, A., Abdulhaq Marraiki, N., El-Zaidy, M., AlSubeie, M.S., 2020. Green biosynthesis of silver nanoparticle using *Commiphora myrrh* extract and evaluation of their antimicrobial activity and colon cancer cells viability. *Journal of King Saud University - Science* 32, 3372–3379. <https://doi.org/10.1016/j.jksus.2020.09.024>.
- Anand, K., Gengan, R.M., Phulukdaree, A., Chuturgoon, A., 2015. Agroforestry waste moringa oleifera petals mediated green synthesis of gold nanoparticles and their anti-cancer and catalytic activity. *J. Ind. Eng. Chem.* 21, 1105–1111. <https://doi.org/10.1016/j.jiec.2014.05.021>.
- Aromal, S.A., Vidhu, V.K., Philip, D., 2012. Green synthesis of well-dispersed gold nanoparticles using *Macrotyloma uniflorum*. *Spectrochimica Acta - Part A: Molecular and Biomolecular Spectroscopy* 85, 99–104. <https://doi.org/10.1016/j.saa.2011.09.035>.
- Aswathy Aromal, S., Philip, D., 2012. Green synthesis of gold nanoparticles using *Trigonella foenum-graecum* and its size-dependent catalytic activity.

- Spectrochim. Acta Part A Mol. Biomol. Spectrosc. 97. <https://doi.org/10.1016/j.saa.2012.05.083>.
- Atta, A.M., Al-Lohedan, H.A., Al-Hussain, S.A., 2014. Synthesis of stabilized myrrh-capped hydrocolloidal magnetite nanoparticles. *Molecules* 19, 11263–11278. <https://doi.org/10.3390/molecules190811263>.
- Aziz, W.J., Mezher, S.J., Muhsien Hassan, M.A., 2015. Gas sensor of Au/AgNPs/PSi/c-Si using pulsed laser ablation using a YAG: Nd laser. *Optik* 126. <https://doi.org/10.1016/j.ijleo.2015.06.033>.
- Balasubramanian, S.K., Yang, L., Yung, L.Y.L., Ong, C.N., Ong, W.Y., Yu, L.E., 2010. Characterization, purification, and stability of gold nanoparticles. *Biomaterials* 31, 9023–9030. <https://doi.org/10.1016/j.biomaterials.2010.08.012>.
- Barai, A.C., Paul, K., Dey, A., Manna, S., Roy, S., Bag, B.G., Mukhopadhyay, C., 2018. Green synthesis of Nerium oleander-conjugated gold nanoparticles and study of its in vitro anticancer activity on MCF-7 cell lines and catalytic activity. *Nano Convergence* 5. <https://doi.org/10.1186/s40580-018-0142-5>.
- Behzad, F., Naghib, S.M., kouhbanani, M.A.J., Tabatabaei, S.N., Zare, Y., Rhee, K.Y., 2021. An overview of the plant-mediated green synthesis of noble metal nanoparticles for antibacterial applications. *J. Ind. Eng. Chem.* 94. <https://doi.org/10.1016/j.jiec.2020.12.005>.
- Ben-Yehoshua, S., Borowitz, C., 2012. Frankincense, Myrrh, and Balm of Gilead: Ancient Spices of Southern Arabia and Judea. *Horticultural Reviews*.
- Bhattacharjee, M.K., Alenezi, T., 2020. Antibiotic in myrrh from *Commiphora molmol* preferentially kills nongrowing bacteria. *Future Sci. OA* 6. <https://doi.org/10.2144/fsoa-2019-0121>.
- Burns, C., Spendel, W.U., Puckett, S., Pacey, G.E., 2006. Solution ionic strength effect on gold nanoparticle color transition. *Talanta* 69, 873–876. <https://doi.org/10.1016/j.talanta.2005.11.038>.
- Cao, B., Wei, X.-C., Xu, X.-R., Zhang, H.-Z., Luo, C.-H., Feng, B., Xu, R.-C., Zhao, S.-Y., Du, X.-J., Han, L., Zhang, D.-K., 2019. Seeing the Unseen of the Combination of Two Natural Resins, Frankincense and Myrrh: Changes in Chemical Constituents and Pharmacological Activities. *Molecules* 24, 3076. <https://doi.org/10.3390/molecules24173076>.
- Chen, H., Kou, X., Yang, Z., Ni, W., Wang, J., 2008. Shape- and size-dependent refractive index sensitivity of gold nanoparticles. *Langmuir* 24, 5233–5237. <https://doi.org/10.1021/la800305j>.
- Chen, J., Li, Y., Fang, G., Cao, Z., Shang, Y., Alfarraj, S., Ali Alharbi, S., Duan, X., Yang, S., Li, J., 2021. Green synthesis, characterization, cytotoxicity, antioxidant, and anti-human ovarian cancer activities of *Curcuma kwangsiensis* leaf aqueous extract green-synthesized gold nanoparticles. *Arabian J. Chem.* 14. <https://doi.org/10.1016/j.arabj.2021.103000>.
- Chen, Y., Zhou, C., Ge, Z., Liu, Y., Liu, Y., Feng, W., Li, S., Chen, G., Wei, T., 2013. Composition and potential anticancer activities of essential oils obtained from myrrh and frankincense. *Oncology Letters* 6, 1140–1146. <https://doi.org/10.3892/ol.2013.1520>.
- Clarance, P., Luvankar, B., Sales, J., Khusro, A., Agastian, P., Tack, J.C., al Khulaifi, M.M., Al-Shwaiman, H.A., Elgorban, A.M., Syed, A., Kim, H.J., 2020. Green synthesis and characterization of gold nanoparticles using endophytic fungi *Fusarium solani* and its in-vitro anticancer and biomedical applications. *Saudi J. Biol. Sci.* 27, 706–712. <https://doi.org/10.1016/j.sjbs.2019.12.026>.
- David, L., Moldovan, B., Vulcu, A., Olenic, L., Perde-Schrepler, M., Fischer-Fodor, E., Florea, A., Crisan, M., Chiorean, I., Clichici, S., Filip, G.A., 2014. Green synthesis, characterization and anti-inflammatory activity of silver nanoparticles using European black elderberry fruits extract. *Colloids Surf., B* 122. <https://doi.org/10.1016/j.colsurfb.2014.08.018>.
- De, M., Ghosh, P.S., Rotello, V.M., 2008. Applications of Nanoparticles in Biology. *Adv. Mater.* 20. <https://doi.org/10.1002/adma.200703183>.
- Desai, M.P., Patil, R., Pawar, K.D., 2020. Green biogenic approach to optimized biosynthesis of noble metal nanoparticles with potential catalytic, antioxidant and antihemolytic activities. *Process Biochem.* 98. <https://doi.org/10.1016/j.procbio.2020.08.005>.
- Dizaj, S.M., Lotfipour, F., Barzegar-Jalali, M., Zarrintan, M.H., Adibkia, K., 2014. Antimicrobial activity of the metals and metal oxide nanoparticles. *Mater. Sci. Eng., C* 44. <https://doi.org/10.1016/j.msec.2014.08.031>.
- Dong, Y.C., Hajfathalian, M., Maidment, P.S.N., Hsu, J.C., Naha, P.C., Si-Mohamed, S., Breuille, M., Kim, J., Chhour, P., Douek, P., Litt, H.I., Cormode, D.P., 2019. Effect of Gold Nanoparticle Size on Their Properties as Contrast Agents for Computed Tomography. *Sci. Rep.* 9. <https://doi.org/10.1038/s41598-019-50332-8>.
- Doroudian, M., O' Neill, A., mac Loughlin, R., Prina-Mello, A., Volkov, Y., Donnelly, S. C., 2021. Nanotechnology in pulmonary medicine. *Curr. Opin. Pharmacol.* 56. <https://doi.org/10.1016/j.coph.2020.11.002>.
- Dreaden, E.C., Alkilany, A.M., Huang, X., Murphy, C.J., El-Sayed, M.A., 2012. The golden age: Gold nanoparticles for biomedicine. *Chem. Soc. Rev.* 41, 2740–2779. <https://doi.org/10.1039/c1cs15237h>.
- Eccles, H., 1999. Treatment of metal-contaminated wastes: why select a biological process? *Trends Biotechnol.* 17. [https://doi.org/10.1016/S0167-7799\(99\)01381-5](https://doi.org/10.1016/S0167-7799(99)01381-5).
- Eid, R.A. et al., 2021. Efficacy of *Commiphora myrrh* mouthwash on early wound healing after tooth extraction: A randomized controlled trial. *Saudi Dental Journal* 33, 44–54. <https://doi.org/10.1016/j.sdentj.2019.11.011>.
- Elia, P., Zach, R., Hazan, S., Kulusheva, S., Porat, Z., Zeiri, Y., 2014. Green synthesis of gold nanoparticles using plant extracts as reducing agents. *Int. J. Nanomed.* 9, 4007–4021. <https://doi.org/10.2147/IJN.S57343>.
- ElMitwalli, O.S., Barakat, O.A., Daoud, R.M., Akhtar, S., Henari, F.Z., 2020. Green synthesis of gold nanoparticles using cinnamon bark extract, characterization, and fluorescence activity in Au/eosin Y assemblies. *J. Nanopart. Res.* 22. <https://doi.org/10.1007/s11051-020-04983-8>.
- Faisal, S., Al-Radadi, N.S., Jan, H., et al., 2021. Curcuma longa Mediated Synthesis of Copper Oxide, Nickel Oxide and Cu-Ni Bimetallic Hybrid Nanoparticles: Characterization and Evaluation for Antimicrobial, Anti-Parasitic and Cytotoxic Potentials. *coatings*, 11, 849. <https://doi.org/10.3390/coatings11070849>.
- Falcaro, P., Ricco, R., Yazdi, A., Imaz, I., Furukawa, S., Maspoth, D., Ameloot, R., Evans, J.D., Doonan, C.J., 2016. Application of metal and metal oxide nanoparticles@MOFs. *Coord. Chem. Rev.* 307. <https://doi.org/10.1016/j.ccr.2015.08.002>.
- Fernández-García, M., Rodríguez, J.A., 2007. Metal Oxide Nanoparticles. BNL-79479-2007-BC.
- Franke, M.E., Koplin, T.J., Simon, U., 2006. Metal and metal oxide nanoparticles in chemiresistors: Does the nanoscale matter? *Small*. <https://doi.org/10.1002/sml.200500261>.
- Gan, N., Sun, Q., Zhao, L., Tang, P., Suo, Z., Zhang, S., Zhang, Y., Zhang, M., Wang, W., Li, H., 2019. Protein corona of metal-organic framework nanoparticles: Study on the adsorption behavior of protein and cell interaction. *Int. J. Biol. Macromol.* 140. <https://doi.org/10.1016/j.ijbiomac.2019.08.183>.
- Guo, Y., Jiang, N., Zhang, L., Yin, M., 2020. Green synthesis of gold nanoparticles from *Fritillaria cirrhosa* and its anti-diabetic activity on Streptozotocin induced rats. *Arabian J. Chem.* 13, 5096–5106. <https://doi.org/10.1016/j.arabj.2020.02.009>.
- Haffor, A.S.A., 2010. Effect of *Commiphora molmol* on leukocytes proliferation in relation to histological alterations before and during healing from injury. *Saudi J. Biol. Sci.* 17, 139–146. <https://doi.org/10.1016/j.sjbs.2010.02.007>.
- Hosseini-mehr, S.J., Mahmouzzadeh, A., Ahmadi, A., Ashrafi, S.A., Shafaghati, N., Hedayati, N., 2011. The Radioprotective Effect of *Zataria multiflora* Against Genotoxicity Induced by g Irradiation g Irradiation in Human Blood Lymphocytes. *CANCER BIOTHERAPY AND RADIOPHARMACEUTICALS*, 26 (3), 325–329. <https://doi.org/10.1089/cbr.2010.0896>.
- Huang, W., Qian, W., El-Sayed, M.A., Ding, Y., Wang, Z.L., 2007. Effect of the lattice crystallinity on the electron-phonon relaxation rates in gold nanoparticles. *J. Phys. Chem. C* 111, 10751–10757. <https://doi.org/10.1021/jp0738917>.
- Hwang, S.J., Jun, S.H., Park, Y., Cha, S.H., Yoon, M., Cho, S., Lee, H.J., Park, Y., 2015. Green synthesis of gold nanoparticles using chlorogenic acid and their enhanced performance for inflammation. *Nanomedicine: Nanotechnology, Biology, and Medicine* 11, 1677–1688. <https://doi.org/10.1016/j.nano.2015.05.002>.
- Jain, P.K., El-Sayed, I.H., El-Sayed, M.A., 2007. Au nanoparticles target cancer. *Nano Today* 2. [https://doi.org/10.1016/S1748-0132\(07\)70016-6](https://doi.org/10.1016/S1748-0132(07)70016-6).
- Kamat, S., Kumari, M., Jayabaskaran, C., 2021. Nano-engineered tools in the diagnosis, therapeutics, prevention, and mitigation of SARS-CoV-2. *J. Control. Release* 338. <https://doi.org/10.1016/j.jconrel.2021.08.046>.
- Kaviya, S., Santhanalakshmi, J., Viswanathan, B., Muthumary, J., Srinivasan, K., 2011. Biosynthesis of silver nanoparticles using citrus sinensis peel extract and its antibacterial activity. *Spectrochimica Acta - Part A: Molecular and Biomolecular Spectroscopy* 79, 594–598. <https://doi.org/10.1016/j.saa.2011.03.040>.
- Khalaf, M.A., Cheah, C.B., Ramli, M., Ahmed, N.M., Al-Shwaiter, A., 2021. Effect of nano zinc oxide and silica on mechanical, fluid transport and radiation attenuation properties of steel furnace slag heavyweight concrete. *Constr. Build. Mater.* 274. <https://doi.org/10.1016/j.conbuildmat.2020.121785>.
- Khalil, N., Fikry, S., Salama, O., 2020. Bactericidal activity of Myrrh extracts and two dosage forms against standard bacterial strains and multidrug-resistant clinical isolates with GC/MS profiling. *AMB Express* 10. <https://doi.org/10.1186/s13568-020-0958-3>.
- Khan, M., Ahmad, F., Koivisto, J.T., Kellomäki, M., 2020. Green synthesis of controlled size gold and silver nanoparticles using antioxidant as capping and reducing agent. *Colloids Interface Sci. Commun.* 39. <https://doi.org/10.1016/j.colcom.2020.100322>.
- Khan, S.H., 2020. Green Nanotechnology for the Environment and Sustainable Development. 13–46. https://doi.org/10.1007/978-3-030-17724-9_2.
- Khandanlou, R., Murthy, V., Saranath, D., Damani, H., 2018. Synthesis and characterization of gold-conjugated *Backhousia citriodora* nanoparticles and their anticancer activity against MCF-7 breast and HepG2 liver cancer cell lines. *J. Mater. Sci.* 53, 3106–3118. <https://doi.org/10.1007/s10853-017-1756-4>.
- Kim, H., seok, Seo, Y.S., Kim, K., Han, J.W., Park, Y., Cho, S., 2016. Concentration Effect of Reducing Agents on Green Synthesis of Gold Nanoparticles: Size, Morphology, and Growth Mechanism. *Nanoscale Res. Lett.* 11. <https://doi.org/10.1186/s11671-016-1393-x>.
- Kiran, M.S., Rajith Kumar, C.R., Shwetha, U.R., Onkarappa, H.S., Betageri, V.S., Latha, M.S., 2021. Green synthesis and characterization of gold nanoparticles from *Moringa oleifera* leaves and assessment of antioxidant, antidiabetic and anticancer properties. *Chem. Data Collect.* <https://doi.org/10.1016/j.cdc.2021.100714>.
- Kumar, K.P., Paul, W., Sharma, C.P., 2011. Green synthesis of gold nanoparticles with Zingiber officinale extract: Characterization and blood compatibility. *Process Biochem.* 46. <https://doi.org/10.1016/j.procbio.2011.07.011>.
- Kumari, P., Meena, A., 2020. Green synthesis of gold nanoparticles from *Lawsonianermis* and its catalytic activities following the Langmuir-Hinshelwood mechanism. *Colloids Surf., A* 606. <https://doi.org/10.1016/j.colsurfa.2020.125447>.
- Kunchandy, E., Rao, M.N.A., 1990. Oxygen radical scavenging activity of curcumin. *Int. J. Pharm.* 58 (3), 237–240. [https://doi.org/10.1016/0378-5173\(90\)90201-E](https://doi.org/10.1016/0378-5173(90)90201-E).
- Lasagna-Reeves, C., Gonzalez-Romero, D., Barria, M.A., Olmedo, I., Clos, A., Sadagopa Ramanujam, V.M., Urayama, A., Vergara, L., Kogan, M.J., Soto, C., 2010. Bioaccumulation and toxicity of gold nanoparticles after repeated

- administration in mice. *Biochem. Biophys. Res. Commun.* 393. <https://doi.org/10.1016/j.bbrc.2010.02.046>.
- Lee, J., Tanaka, T., Lee, J., Mori, H., 2007. Effect of substrates on the melting temperature of gold nanoparticles. *CALPHAD: Comput. Coupling Phase Diagrams Thermochem.* 31, 105–111. <https://doi.org/10.1016/j.calphad.2006.10.001>.
- Lee, K.X., Shamelii, K., Yew, Y.P., Teow, S.Y., Jahangirian, H., Raffee-Moghaddam, R., Webster, T.J., 2020. Recent developments in the facile bio-synthesis of gold nanoparticles (AuNPs) and their biomedical applications. *Int. J. Nanomed.* <https://doi.org/10.2147/IJN.S233789>.
- Lee, T.Y., Lam, T.H., 1993. Allergic contact dermatitis due to a Chinese orthopaedic solution Tieh Ta Yao Gin. *Contact Dermatitis* 28. <https://doi.org/10.1111/j.1600-0536.1993.tb03348.x>.
- Li, Y., Li, J., Ding, J., Song, Z., Yang, B., Zhang, C., Guan, B., 2022. Degradation of nano-sized polystyrene plastics by ozonation or chlorination in drinking water disinfection processes. *Chem. Eng. J.* 427. <https://doi.org/10.1016/j.cej.2021.131690>.
- Liang, J., Liang, K., 2021. Nano-bio-interface engineering of metal-organic frameworks. *Nano Today* 40. <https://doi.org/10.1016/j.nantod.2021.101256>.
- Liao, X., Pu, Y., Zhu, D., 2021. Synergistic effect of co-doping of nano-sized ZnO and Nb2O5 on the enhanced nonlinear coefficient of TiO2 varistor with low breakdown voltage. *J. Alloy. Compd.* 886. <https://doi.org/10.1016/j.jallcom.2021.161170>.
- Link, S., El-Sayed, M.A., 1999. Size and temperature dependence of the plasmon absorption of colloidal gold nanoparticles. *J. Phys. Chem. B* 103, 4212–4217. <https://doi.org/10.1021/jp984796o>.
- Liu, Y., Huang, W., Chen, W., Wang, X., Guo, J., Tian, H., Zhang, H., Wang, Y., Yu, B., Ren, T.-L., Xu, J., 2019. Plasmon resonance enhanced WS2 photodetector with ultra-high sensitivity and stability. *Appl. Surf. Sci.* 481. <https://doi.org/10.1016/j.apsusc.2019.03.179>.
- Llop, J., Estrela-Lopis, I., Ziolo, R.F., González, A., Fleddermann, J., Dorn, M., Vallejo, V. G., Simon-Vazquez, R., Donath, E., Mao, Z., Gao, C., Moya, S.E., 2014. Uptake, Biological Fate, and Toxicity of Metal Oxide Nanoparticles. *Part. Part. Syst. Char.* 31, 24–35. <https://doi.org/10.1002/ppsc.201300323>.
- Mai, X.T., Tran, M.C., Hoang, A.Q., Nguyen, P.D.N., Nguyen, T.H., Tran, H.N., Nguyen, P.T., 2021. Gold nanoparticles from *Celastrus hindsii* and HAuCl4: Green synthesis, characteristics, and their cytotoxic effects on HeLa cells. *Green Process. Synth.* 10, 73–84. <https://doi.org/10.1515/gps-2021-0009>.
- Malathi, S., Balakumaran, M.D., Kalaichelvan, P.T., Balasubramanian, S., 2013. Green synthesis of gold nanoparticles for controlled delivery. *Advanced Materials Letters* 4, 933–940. <https://doi.org/10.5185/amlett.2013.5477>.
- Mironava, T., Hadjiargyrou, M., Simon, M., Jurukovski, V., Rafailovich, M.H., 2010. Gold nanoparticles cellular toxicity and recovery: Effect of size, concentration and exposure time. *Nanotoxicology* 4, 120–137. <https://doi.org/10.3109/17435390903471463>.
- Naem, G.A., Jaloot, A.S., Owaid, M.N., Muslim, R.F., 2021. Green synthesis of gold nanoparticles from *Coprinus comatus*, *agaricaceae*, and the effect of ultraviolet irradiation on their characteristics. *Walailak Journal of Science and Technology*, 18. <https://doi.org/10.48048/wjst.2021.9396>.
- Narayanan, K.B., Sakthivel, N., 2011. Extracellular synthesis of silver nanoparticles using the leaf extract of *Coleus amboinicus* Lour. *Mater. Res. Bull.* 46, 1708–1713. <https://doi.org/10.1016/j.materresbull.2011.05.041>.
- Negahdari, S., Galehdari, H., Kesmati, M., Rezaie, A., Shariati, G., 2017. Wound healing activity of extracts and formulations of Aloe vera, henna, *Adiantum capillus-veneris*, and myrrh on mouse dermal fibroblast cells. *International Journal of Preventive Medicine* 8. https://doi.org/10.4103/ijpvm.IJPVM_338_16.
- Neha, R., Adithya, S., Jayaraman, R.S., Gopinath, K.P., M, P., L. P., Arun, J., 2021. Nanoadsorbents an effective candidate for removal of toxic pharmaceutical compounds from aqueous environment: A critical review on emerging trends. *Chemosphere* 272. <https://doi.org/10.1016/j.chemosphere.2021.129852>.
- Nikam, A., v., Prasad, B.L.V., Kulkarni, A.A., 2018. Wet chemical synthesis of metal oxide nanoparticles: A review. *CrystEngComm* 20, 5091–5107. <https://doi.org/10.1039/C8CE00487K>.
- Nirmala Grace, A., Pandian, K., 2007. Antibacterial efficacy of aminoglycosidic antibiotics protected gold nanoparticles—A brief study. *Colloids Surf., A* 297. <https://doi.org/10.1016/j.colsurfa.2006.10.024>.
- Okitsu, K., Sharyo, K., Nishimura, R., 2009. One-pot synthesis of gold nanorods by ultrasonic irradiation: The effect of pH on the shape of the gold nanorods and nanoparticles. *Langmuir* 25, 7786–7790. <https://doi.org/10.1021/la9017739>.
- Parida, U.K., Biswal, S.K., Bindhani, B.K., 2014. Green Synthesis and Characterization of Gold Nanoparticles: Study of Its Biological Mechanism in Human SUDHL-4 Cell Line. *Advances in Biological Chemistry* 04, 360–375. <https://doi.org/10.4236/abc.2014.46041>.
- Perveen, K., Husain, F.M., Qais, F.A., Khan, A., Razak, S., Afsar, T., Alam, P., Almajwal, A.M., Abulmeaty, M.M.A., 2021. Microwave-assisted rapid green synthesis of gold nanoparticles using seed extract of *trachyspermum ammi*: Ros mediated biofilm inhibition and anticancer activity. *Biomolecules* 11, 1–16. <https://doi.org/10.3390/biom11020197>.
- Qiu, F., Zhang, H., Li, C.-L., Wang, Z.-F., Chang, F., Yang, H.-Y., Li, C.-D., Han, X., Jiang, Q.-C., 2021. Simultaneously enhanced strength and toughness of cast medium carbon steels matrix composites by trace nano-sized TiC particles. *Mater. Sci. Eng., A* 819. <https://doi.org/10.1016/j.msea.2021.141485>.
- Rajeshkumar, S., Bharath, L.V., 2017. Mechanism of plant-mediated synthesis of silver nanoparticles – A review on biomolecules involved, characterisation and antibacterial activity. *Chem. Biol. Interact.* 273. <https://doi.org/10.1016/j.cbi.2017.06.019>.
- Raliya, R., Saha, D., Chadha, T.S., Raman, B., Biswas, P., 2017. Non-invasive aerosol delivery and transport of gold nanoparticles to the brain. *Sci. Rep.* 7. <https://doi.org/10.1038/srep44718>.
- Ramakrishna, M., Rajesh Babu, D., Gengan, R.M., Chandra, S., Nageswara Rao, G., 2016. Green synthesis of gold nanoparticles using marine algae and evaluation of their catalytic activity. *Journal of Nanostructure in Chemistry* 6, 1–13. <https://doi.org/10.1007/s40097-015-0173-y>.
- Richter, K., Birkner, A., Mudring, A.-V., 2010. Stabilizer-Free Metal Nanoparticles and Metal-Metal Oxide Nanocomposites with Long-Term Stability Prepared by Physical Vapor Deposition into Ionic Liquids. *Angew. Chem. Int. Ed.* 49. <https://doi.org/10.1002/anie.200901562>.
- Satpathy, S., Patra, A., Ahirwar, B., Hussain, M.D., 2020. Process optimization for green synthesis of gold nanoparticles mediated by extract of *Hygrophila spinosa* T. In: *Anders and their biological applications. Physica E: Low-dimensional Systems and Nanostructures* 121. <https://doi.org/10.1016/j.physe.2019.113830>.
- Sengupta, M., Pal, R., Nath, A., Chakraborty, B., Singh, L.M., Das, B., Ghosh, S.K., 2018. Anticancer efficacy of noble metal nanoparticles relies on reprogramming tumor-associated macrophages through redox pathways and pro-inflammatory cytokine cascades. *Cell. Mol. Immunol.* <https://doi.org/10.1038/s41423-018-0046-7>.
- Senthilkumar, P., Surendran, L., Sudhagar, B., Kumar, R.S., D.s., 2019. Facile green synthesis of gold nanoparticles from marine algae *Gelidium acerosa* and evaluation of its biological Potential. *SN Applied Sciences* 1. <https://doi.org/10.1007/s42452-019-0284-z>.
- Sheir, Z., Nasr, A.A., Massoud, A., Salama, O., Badra, G.A., El-Shennawy, H., Hassan, N., Hammad, S.M., 2001. A safe, effective, herbal antischistosomal therapy derived from myrrh. *Am. J. Trop. Med. Hyg.* 65, 700–704. <https://doi.org/10.4269/ajtmh.2001.65.700>.
- Shejwal, K.P., Randive, D.S., Bhinge, S.D., Bhutkar, M.A., Todkar, S.S., Mulla, A.S., Jadhav, N.R., 2021. Green synthesis of silver, iron and gold nanoparticles of lycopene extracted from tomato: their characterization and cytotoxicity against COLO320DM, HT29 and Hella cell. *J. Mater. Sci. - Mater. Med.* 32. <https://doi.org/10.1007/s10856-021-06489-8>.
- Siegel, J., Kolářová, K., Vosmanská, V., Rimpelová, S., Leitner, J., Švorčík, V., 2013. Antibacterial properties of green-synthesized noble metal nanoparticles. *Mater. Lett.* 113. <https://doi.org/10.1016/j.matlet.2013.09.047>.
- Singh, A.K., Srivastava, O.N., 2015. One-Step Green Synthesis of Gold Nanoparticles Using Black Cardamom and Effect of pH on Its Synthesis. *Nanoscale Res. Lett.* 10. <https://doi.org/10.1186/s11671-015-1055-4>.
- Singh, A.K., Tiwari, R., Singh, V.K., Singh, P., Khadim, S.R., Singh, U., Laxmi, S., V., Hasan, S.H., Asthana, R.K., 2019. Green synthesis of gold nanoparticles from *Dunalialla salina*, its characterization and in vitro anticancer activity on breast cancer cell line. *J. Drug Delivery Sci. Technol.* 51. <https://doi.org/10.1016/j.jddst.2019.02.023>.
- Singh, P., Ahn, S., Kang, J.P., Veronika, S., Huo, Y., Singh, H., Chokkaligam, M., El-Agamy Farh, M., Aceituno, V.C., Kim, Y.J., Yang, D.C., 2018. In vitro anti-inflammatory activity of spherical silver nanoparticles and monodisperse hexagonal gold nanoparticles by fruit extract of *Prunus serrulata*: a green synthetic approach. *Artif. Cells Nanomed. Biotechnol.* 46, 2022–2032. <https://doi.org/10.1080/21691401.2017.1408117>.
- Slocik, J.M., Zabinski, J.S., Phillips, D.M., Naik, R.R., 2008. Colorimetric response of peptide-functionalized gold nanoparticles to metal ions. *Small* 4, 548–551. <https://doi.org/10.1002/sml.200700920>.
- Sonavane, G., Tomoda, K., Sano, A., Ohshima, H., Terada, H., Makino, K., 2008. In vitro permeation of gold nanoparticles through rat skin and rat intestine: Effect of particle size. *Colloids Surf., B* 65, 1–10. <https://doi.org/10.1016/j.colsurfb.2008.02.013>.
- Sperling, R.A., Gil, P.R., Zhang, F., Zanella, M., Parak, W.J., 2008. Biological applications of gold nanoparticles. *Chem. Soc. Rev.* 37, 1896–1908. <https://doi.org/10.1039/b712170a>.
- Stoimenov, P.K., Klingner, R.L., Marchin, G.L., Klabunde, K.J., 2002. Metal oxide nanoparticles as bactericidal agents. *Langmuir* 18, 6679–6686. <https://doi.org/10.1021/la0202374>.
- Su, S., Wang, T., Duan, J.-A., Zhou, W., Hua, Y.-Q., Tang, Y.-P., Yu, L., Qian, D.-W., 2011. Anti-inflammatory and analgesic activity of different extracts of *Commiphora myrrha*. *J. Ethnopharmacol.* 134. <https://doi.org/10.1016/j.jep.2010.12.003>.
- Sun, L., Zhang, Z., Wang, S., Zhang, J., Li, H., Ren, L., Weng, J., Zhang, Q., 2009. Effect of pH on the interaction of gold nanoparticles with DNA and application in the detection of human p53 gene mutation. *Nanoscale Res. Lett.* 4, 216–220. <https://doi.org/10.1007/s11671-008-9228-z>.
- Udayasoorian, C., Kumar, K.V., Jayabalakrishnan, R.M., 2011. EXTRACELLULAR SYNTHESIS OF SILVER NANOPARTICLES USING LEAF EXTRACT OF CASSIA AURICULATA. *Digest Journal of Nanomaterials and Biostructures.*
- Umamaheswari, C., Lakshmanan, A., Nagarajan, N.S., 2018. Green synthesis, characterization and catalytic degradation studies of gold nanoparticles against congo red and methyl orange. *J. Photochem. Photobiol., B* 178, 33–39. <https://doi.org/10.1016/j.jphotobiol.2017.10.017>.
- Vijayakumar, S., Vinayagam, R., Anand, M.A.V., Venkatachalam, K., Saravanakumar, K., Wang, M.H., Casimeer, C., S., KM, G., David, E., 2020. Green synthesis of gold nanoparticle using *Eclipta alba* and its antidiabetic activities through regulation of Bcl-2 expression in pancreatic cell line. *J. Drug Delivery Sci. Technol.* 58. <https://doi.org/10.1016/j.jddst.2020.101786>.
- Walsh, M.E., Reis, D., Jones, T., 2010. Integrating complementary and alternative medicine: Use of myrrh in wound management. *Journal of Vascular Nursing* 28, 102. <https://doi.org/10.1016/j.jvn.2010.06.001>.

- Wang, L., Xu, J., Yan, Y., Liu, H., Karunakaran, T., Li, F., 2019. Green synthesis of gold nanoparticles from *Scutellaria barbata* and its anticancer activity in pancreatic cancer cell (PANC-1). *Artif. Cells Nanomed. Biotechnol.* 47, 1617–1627. <https://doi.org/10.1080/21691401.2019.1594862>.
- Wijesekera, R.O.B., 2016. Forest Wealth and Global Health, Wijesekera. *Journal of Tropical Forestry and Environment*.
- Willian, N., Syukri, S., Zulhadjri, Z., Arief, S., 2021. Marine plant mediated green synthesis of silver nanoparticles using mangrove *Rhizophora stylosa*: Effect of variable process and their antibacterial activity. *F1000Research* 10, 768. <https://doi.org/10.12688/f1000research.54661.1>.
- Wink, D.A., Mitchell, J.B., 1998. Chemical biology of nitric oxide: insights into regulatory, cytotoxic, and cytoprotective mechanisms of nitric oxide. *Free Radical Biol. Med.* 25. [https://doi.org/10.1016/S0891-5849\(98\)00092-6](https://doi.org/10.1016/S0891-5849(98)00092-6).
- Wu, C.-C., Chen, D.-H., Org, W.G., 2010. Facile green synthesis of gold nanoparticles with gum arabic as a stabilizing agent and reducing agent. *Gold Bull.*
- xue, Z., He, N., Rao, H., Hu, C., Wang, X., Wang, H., Liu, X., Lu, X., 2017. A green synthetic strategy of nickel hexacyanoferrate nanoparticles supported on the graphene substrate and its non-enzymatic amperometric sensing application. *Appl. Surf. Sci.* 396. <https://doi.org/10.1016/j.apsusc.2016.10.185>.
- Yang, A., Huang, Z., Zhu, Y., Han, Y., Tong, Z., 2021. Preparation of nano-sized calcium carbonate in solution mixing process. *J. Cryst. Growth* 571. <https://doi.org/10.1016/j.jcrysgro.2021.126247>.
- Yang, X., Gao, H., Zhao, L., Wang, T., Sun, P., Liu, F., Lu, G., 2018. Enhanced gas sensing properties of monodisperse Zn₂SnO₄ octahedron functionalized by PdO nanoparticles. *Sens. Actuators, B* 266. <https://doi.org/10.1016/j.snb.2018.03.121>.
- Yas, R.M., Ghafoor, A., Saeed, A., 2021. Anticancer Effect of Green Synthesized Gold Nanoparticles Using Orchid Extract and their Characterizations on Breast Cancer AMJ-13 Cell Line. *Syst. Rev. Pharm.*
- Yue, T., Liu, J., Yang, Y., Chen, S., 2021. Feasibility of cleaning As- and U-containing soil of a gold mine by using biologically nano-sized FeS: Implications for soil remediation technology. *Environ. Technol. Innovation* 23. <https://doi.org/10.1016/j.eti.2021.101775>.
- Zhang, H., Jiang, X., Cao, G., Zhang, X., Croley, T.R., Wu, X., Yin, J.-J., 2018. Effects of noble metal nanoparticles on the hydroxyl radical scavenging ability of dietary antioxidants. *J. Environ. Sci. Health, Part C* 36. <https://doi.org/10.1080/10590501.2018.1450194>.
- Zhang, X., Fan, L., Cui, Y., Cui, T., Chen, S., Ma, G., Hou, W., Wang, L., 2020. Green Synthesis of Gold Nanoparticles Using Longan Polysaccharide and their Reduction of 4-nitrophenol and Biological Applications. *NANO* 15. <https://doi.org/10.1142/S1793292020500022>.
- Zhang, Y., Shareena Dasari, T.P., Deng, H., Yu, H., 2015. Antimicrobial Activity of Gold Nanoparticles and Ionic Gold. *J. Environ. Sci. Health - Part C Environ. Carcinogenesis Ecotoxicol. Rev.* 33, 286–327. <https://doi.org/10.1080/10590501.2015.1055161>.
- Zhao, G., Ran, X., Zhou, X., Tan, X., Lei, H., Xie, X., Yang, L., Du, G., 2018. Green Synthesis of Hydroxylatopillar[5]arene-Modified Gold Nanoparticles and Their Self-Assembly, Sensing, and Catalysis Applications. *ACS Sustainable Chem. Eng.* 6, 3938–3947. <https://doi.org/10.1021/acssuschemeng.7b04292>.
- Zhou, Q., Wei, T., Liu, Z., Zhang, L., Yuan, B., Fan, Z., 2019. Nickel hexacyanoferrate on graphene sheets for high-performance asymmetric supercapacitors in neutral aqueous electrolyte. *Electrochim. Acta* 303. <https://doi.org/10.1016/j.electacta.2019.02.070>.
- Cruciani, R.A., Barker, J.L., Zasloff, M., et al., 1991. Antibiotic magainins exert cytolytic activity against transformed cell lines through channel formation. *Proc. Natl. Acad. Sci. U. S. A.* 88, 3792–3796.
- El-Adl, K., Ibrahim, M.K., Khedr, F., et al., 2021. N-Substituted-4-phenylphthalazin-1-amine-derived VEGFR-2 inhibitors: design, synthesis, molecular docking, and anticancer evaluation studies. *Arch. Pharm.* 354, 2000219.
- Karim, N., Khan, I., Khan, W., et al., 2019. Anti-nociceptive and Anti-inflammatory Activities of Asparacosin A Involve Selective Cyclooxygenase 2 and Inflammatory Cytokines Inhibition: An in-vitro, in-vivo, and in-silico Approach. *Front. Immunol.* 10. <https://doi.org/10.3389/fimmu.2019.00581>.
- Mai, J.C., Mi, Z., Kim, S.-H., et al., 2001. A proapoptotic peptide for the treatment of solid tumors. *Cancer Res.* 61, 7709–7712.
- Missioui, M., Mortada, S., Guerrab, W., et al., 2021. Novel antioxidant quinoxaline derivative: Synthesis, crystal structure, theoretical studies, antidiabetic activity and molecular docking study. *J. Mol. Struct.* 1239. <https://doi.org/10.1016/j.molstruc.2021.130484>.
- Miyazaki, Y., Matsunaga, S., Tang, J., et al., 2005. Novel 4-amino-furo[2,3-d]pyrimidines as Tie-2 and VEGFR2 dual inhibitors. *Bioorg. Med. Chem. Lett.* 15, 2203–2207. <https://doi.org/10.1016/j.bmcl.2005.03.034>.
- Rimon, G., Sidhu, R.S., Lauver, D.A., et al., 2010. Coxibs interfere with the action of aspirin by binding tightly to one monomer of cyclooxygenase-1. *Proc. Natl. Acad. Sci.* 107, 28–33. <https://doi.org/10.1073/pnas.0909765106>.
- Roig-Zamboni, V., Cobucci-Ponzano, B., Iacono, R., et al., 2017. Structure of human lysosomal acid α -glucosidase—a guide for the treatment of Pompe disease. *Nat. Commun.* 8, 1111. <https://doi.org/10.1038/s41467-017-01263-3>.
- Schrödinger Suite 2021-2. New York, NY, Schrödinger, LLC (2021).
- Tian, M.Y., Zhang, X.F., Xie, L., et al., 2008. The effect of Cu²⁺ on the interaction between an antitumor drug—mitoxantrone and human serum albumin. *J. Mol. Struct.* 892, 20–24.
- Wang, J.L., Limburg, D., Graneto, M.J., et al., 2010. The novel benzopyran class of selective cyclooxygenase-2 inhibitors. Part 2: The second clinical candidate having a shorter and favorable human half-life. *Bioorg. Med. Chem. Lett.* 20, 7159–7163. <https://doi.org/10.1016/j.bmcl.2010.07.054>.
- Williams, L.K., Li, C., Withers, S.G., et al., 2012. Order and Disorder: Differential Structural Impacts of Myricetin and Ethyl Caffeate on Human Amylase, an Antidiabetic Target. *J. Med. Chem.* 55, 10177–10186. <https://doi.org/10.1021/jm301273u>.